ISTANBUL TECHNICAL UNIVERSITY ★ GRADUATE SCHOOL

SILK FIBROIN CRYOGEL-BASED SHAPE MEMORY ORGANOHYDROGELS

M. Sc. THESIS

YAHYA BAŞ

Department of Polymer Science and Technology

Polymer Science and Technology Programme

Thesis Advisor: Prof. Dr. Oğuz OKAY

AUGUST 2022

İSTANBUL TEKNİK ÜNİVERSİTESİ ★ LİSANSÜSTÜ EĞİTİM ENSTİTÜSÜ

İPEK FİBROİN KRİYOJEL BAZLI ŞEKİL HAFIZALI ORGANOHİDROJELLER

YÜKSEK LİSANS TEZİ

YAHYA BAŞ
(515191025)

Polimer Bilim ve Teknolojisi Anabilim Dalı

Polimer Bilim ve Teknolojisi Programı

Tez Danışmanı: Prof. Dr. Oğuz OKAY

AĞUSTOS 2022

Yahya BAŞ, an M. Sc. Student of ITU Graduate School, student ID 515191025, successfully defended the thesis entitled “SILK FIBROIN CRYOGEL-BASED SHAPE MEMORY ORGANOHYDROGELS”, which he prepared after fulfilling the requirements specified in the associated legislations, before the jury whose signatures are below.

Thesis Advisor :	**Prof. Dr. Oguz OKAY** İstanbul Technical University	.....
Jury Members :	**Assoc. Prof. Dr. Bünyamin KARAGÖZ** Istanbul Technical University	.....
	Assoc. Prof. Dr. Deniz CEYLAN TUNCABOYLU Bezmialem Vakif Universtiy	.....

Date of Submission : 12.08.2022
Date of Defense : 19.08.2022

To my parents, my teachers, my friends… To all who inspired and assisted me to pursue my dreams,

To Gülşah above all. My biggest dream.

FOREWORD

Pursuing dreams is what gives our lives meaning. It is worth all the pain, suffering, and sacrifices along the way. And achieving this conclusion is what makes me think of the process behind it. I have many thanks for giving.

First thing, I would like to express my gratitude to my wise and doyen advisor Prof. Dr. Oğuz OKAY. In many ways, he gave me a scientific perspective, he was a living example of the necessity of perfectionism in science. I consider this Master's education the onset of my academic career, and I have learned the way from the very best. Also, I need to express my greetings to Dr. Berkant YETİŞKİN for his caring effort and priceless guidance. In a way, I was his proud 'padawan' and he led me the way to the gates of my Master's journey smoothly and safely. Thank you Dr. YETİŞKİN.

It was my privilege to be among the members of the ITU Polymeric Gels Research Group. I have sent many of them off their journeys, and with the ones remaining with me until now, I wish the very, very best to all of them along their careers and lives. Ç. Buse ORAL, Dr. Burak TAVŞANLI, Özge AKÇA, Sümeyye ÖZER, Gamze DÖŞER, Dr. Turdimuhammad ABDULLAH… Thank you all very much for your help and contribution.

It was my dream to be an ITU student and now I am becoming an alumnus of it. I know my friends, with who I have shared the ideal of ITU education once, are happy and grateful for me. So, my precious friends… This one is for you, too. Thanks for being my brothers for a lifetime.

And there are the ones who gave me this ideal and encoureged me through my life to pursue my dreams. My loved ones. My family. My life's biggest achievement is to see the pride in your eyes and my biggest luck is to feel the depth of your love. Thank you for making me myself by being yourselves. I owe you everything.

I met my miracle in the two and a half years I spent in ITU. She blessed my life with her gracious presence and for that, I will be her admirer all my life. Gülşah, my love… Thank you for being yourself and always being there for me. I love you.

I want to thank the Scientific and Technical Research Council of Turkey (TUBITAK) (Project No. 121Z568) for the financial and material aid they provided for my work.

A final reminder for myself: *They said: "Glory to Thee, of knowledge We have none, save what Thou Hast taught us: In truth it is Thou Who art perfect in knowledge and wisdom."* (The Qur'an, 2:32)

July 2022

Yahya BAŞ
Chemical Engineer

TABLE OF CONTENTS

Page

ABBREVATIONS

SF	**:** Silk fibroin
OHG	**:** Organohydrogel
AAc	**:** Acrylic Acid
C18A	**:** n-Octadecyl Acrylate
Gly	**:** Glycine
Ala	**:** Alaine
Ser	**:** Serine
H-Bonds	**:** Hydrogen Bonds
pH	**:** Potential of Hydrogen
BDDE	**:** 1,4-Butanediol diglycidyl ether
TEMED	**:** *N,N,N′,N′*-Tetramethylethylenediamine
BAAm	**:** *N,N'*-Methylenebis(acrylamide)
AIBN	**:** *α,α′*-Azoisobutyronitrile
PEG	**:** Poly(ethylene glycol)
ATR-FTIR	**:** Attenuated Total Reflection – Fourier Transform Infrared
XRD	**:** X-Ray Diffraction
DSC	**:** Differantial Scanning Calorimetry
SEM	**:** Scanning Electron Microscopy
MPa	**:** Megapascal
kPa	**:** Kilopascal

SYMBOLS

C_{SF}	: Silk fibroin concentration
x_{C18A}	: C18A mole fraction
q_w, q_v	: Swelling by mass and volume ratios
P%	: Percent porosity
m, m_0, m_{dry}	: Swollen, post-synthesis and dry gel masses
D, D_0, D_{dry}	: Swollen, post-synthesis and dry gel diameters
W_g	: Gel fraction
$q_{w,o}$	: Swelling ratio of cryogel by mass in the monomer solution
$w_{organogel}$	: Mass fraction of organogel in the OHG
w_{C18A}	: Mass fraction of C18A in the OHG
m_{C18A}	: Mass fraction of C18A in the monomer mixture
f_{cry}	: Degree of crystallization
ΔH_m	: Melting enthalpy
E	: Young's modulus
ε, ε_f, ε_{max}	: Strain, fracture strain and maximum strain
σ_{nom}, σ_{true}, σ_f	: Nominal stress, true stress and fracture stress
T_m, T_c	: Melting and crystallization temperature
W	: Toughness
ω	: Angular frequency
γ_0	: Rotational strain
θ_0,θ_d,θ_f,θ_r	: Initial, deformed, fixed and recovered angles
tanδ	: Dissipation factor
U_{hys}	: Hysteresis energy
R_f, R_r	: Shape fixity and recovery ratios

LIST OF TABLES

Page

LIST OF FIGURES

Page

SILK FIBROIN CRYOGEL BASED SHAPE MEMORY ORGANOHYDROGELS

SUMMARY

From textile fibers to biotechnology, silk has been a pivotal material for humanity for centuries. Fibroin, one of the two proteins that consist of silk, facilitates the structural integrity and physical endurance of the silk fibers and has been isolated and widely used for several purposes with its features like hydrophilicity, biocompatibility, and mechanical robustness.

Polymeric gels are polymer-based, crosslinked wet and soft materials, including pore walls spaced by solvents that dissolve the polymer. Regarding the solvent-separator type that they include, the polymeric gels are mainly categorized into three types: hydrogels, organogels, and aerogels and they include water, organic solvents, and air in their pores, respectively. Hydrogels consist of over 90% water in their structure, most of all, possess unparalleled biomimicry due to their hydrophilic nature.

Cryogels are a subclass of hydrogels that are synthesized under 'cryogenic' conditions, meaning under the freezing temperature of the water. Contrary to the conventional hydrogel case, the reason that gelation reaction occurs here is not the heat given to the system, rather it is the increased concentration of gel components in the unfrozen high concentration channels in the reaction system. This influence is called the 'cryo-concentration effect'. This effect provides the cryogels with more reliable mechanical performance and a strictly ordered porous structure that conventional hydrogels lack. Also, the porous morphology of the cryogels mimics the natural extracellular matrix structure of the animals perfectly, according to the scanning electron microscopy (SEM) image comparison of acellularized tissue scaffold and cryogels.

Like there are conventional covalent crosslinks between the polymer chains of polymeric gels, there can also be some secondary interactions whose impact becomes significant upon an increased number of them. They regulate the chain conformation with various bindings they form out of many electrostatic interactions. These switchable crosslinks give the materials adjustable mechanical properties, fixing temporary shapes and healing the defects in their structure. The materials having such properties are called 'smart materials'. Smart materials have a variety of application areas such as sustained drug release systems, nanorobotics, biosensors, and tissue engineering.

In the scope of this thesis, it was aimed to form an interconnected micro-organogel structure made of n-Octadecyl acrylate (C18A) and acrylic acid (AAc) monomers, within the pores of silk fibroin cryogels which are freeze-dried and swollen in an organogel precursor solution. The effect provides the OHGs their smart material abilities are the reversible dissipation and assembling of crystalline domains formed by the long alkyl tails of C18A monomers, with the repelling influence of water surrounding them and the hydrophobic interactions between them. These weak bonds would disappear upon heat exposure, over the melting temperature of poly(C18A) crystallites, around 50 ^{o}C, and would be reformed after the materials cooled down. These switchable crosslinks should provide the OHGs with their altering mechanical (softening and reformability) and shape memory properties.

To confirm these assumptions, two sets of samples were prepared and tested. One set of OHG was made of constant fibroin concentration (5 w/v %) cryogel templates and embedded with micro-organogel structures including 4 different C18A monomer mole fractions: 10, 20, 25, and 30 %. The other set of OHG consisted of 4 different fibroin concentration cryogels: 5, 10, 15, and 20 w/v% scaffolds, and each one was filled with the organogel that has a 30% mole fraction C18A. The questioned parameters in each OHG set were the influence of the C18A mole fraction of organogel and fibroin concentration of cryogel, respectively.

Initially, cryogel templates having 4 different fibroin concentrations were characterized regarding their swelling properties, pore morphologies and sizes, and uniaxial compression mechanical behavior. It was observed that cryogel porosity has decreased from 92 % to 74% with increasing fibroin concentration from 5 w/v% to 20 w/v%. SEM visualization showed that the average pore diameter decreased from 25.7 μm to 16.8 μm. Fourier Transform Infrared Spectrophotometry (FT-IR) results indicated a 10 % increase in the β-sheet conformation ratio.

After the freeze-drying and organogel synthesis within, the OHG porosity was decreased to 45-8 %. The calculated specific pore volume was 17.3 – 2.9 mL/g for cryogels and it was also decreased to a minimum of 0.16 mL/g for OHGs. While Young's modulus was calculated as 0.04 MPa for 5 w/v% cryogels, regarding the increased fibroin concentration and C18A mole fraction, it was raised to a maximum of 17.7 MPa for OHGs with fibroin concentration of 20 w/v%, and C18A mole fraction of 30%. Fracture strains were observed as 10 % lower for the cryogels that became OHGs, while the fracture stresses increased 10 times their initial values.

OHGs were subjected to differential scanning calorimetry (DSC) and rheometer tests to investigate this affiliation between temperature and material properties. In DSC testing, the materials were heated up from 0 to 80 ^{o}C in two cycles. The melting peaks observed around 54 ^{o}C during the heating stage of the test and the crystallization peak at 43 ^{o}C during the cooling stage were attributed to the reversible dissipation and regeneration of poly(C18A) crystallites. The first series of OHGs indicated that the increased mole fraction of C18A has increased the number of secondary interactions. This effect was comparatively shown between OHGs with the aid of a parameter called crystallinity index (f_{cry}) which was calculated from the area below the melting peaks of crystallites in the heating stage of DSC tests. f_{cry} describes the fraction of C18A monomers that contributed to the formation of poly(C18A) crystallites. The f_{cry} values that were calculated regarding the melting enthalpies have shown a drop from 15.7 to 2 % when the C18A mole fractions were decreased from 30 to 10%. As a consequence of the bending shape memory tests, also, the OHGs with maximum C18A mole fractions have been seen to be perfectly capable of keeping the shape dictated to them, whereas OHGs with minimum C18A mole fractions were not.

The second series of OHGs indicated that, with increasing fibroin concentration and cryogel pores getting narrower, the amount of secondary interactions within the micro-

organogel structure gets lower. The calculated f_{cry} values got decreased from 15.7 to 2.9 % with increasing fibroin concentration, from 5 to 20 w/v%.

The morphology of cryogels and OHGs was investigated with X-Ray Diffraction (XRD) tests. Growth and sharpening of the peaks corresponding to $2\theta = 9.5^o$, 20^o, 24.6^o angles with increasing fibroin concentration in cryogels revealed an increase in regular formations such as β-sheets. In the XRD patterns of OHGs, $2\theta = 21.6^o$ peaks, which are not seen in cryogels and correspond to the $d = 0.41$ nm range, revealed that C18A crystallites were formed in the structure. It is thought that the reduction of these peaks with increasing fibroin concentration is due to the difficulty of the orientation required for the formation of crystalline domains in the narrowing pores.

Rheometer measurements done with OHGs with 5 w/v% fibroin and 30% C18A mole fraction have exhibited a significant drop in the elastic modulus (G') of the material, from 1.5 MPa to 220 kPA between room temperature and heated to 65 ^{o}C state. Once the material cooled down to room temperature again, it recovered its initial G' value, which indicated the existence of the reversibly dissipated and reformed crystalline domains. These results indicated the OHG's reversibly adjustable viscoelastic properties with the influence of heat. Also, all OHG's synthesized have exhibited shape memory capability with around 95% shape recovery ratio each.

İPEK FİBROİN KRİYOJEL BAZLI ŞEKİL HAFIZALI ORGANOHİDROJELLER

ÖZET

İpek, binyıllardır süregelen kullanımıyla insanoğlunun faydalandığı en kadim malzemelerden biridir. Dünya medeniyetine sayısız katkıları olmuş, kültürler ve coğrafyalar arası köprüler kurmuş ipeğin serüveni, tarihin akışı ile de farklı bir hal almış, gelişen kimya ve malzeme teknikleri bu doğal polimerin yüksek teknoloji uygulamalarına zemin hazırlamış ve onu bambaşka platformlarda insanlığın faydasına sunmuştur. İpek yapısını oluşturan iki proteinden biri olan fibroin, ipek liflerine yapısal bütünlük ve mekanik mukavemet kazandıran doğal bir biyopolimerdir. Tabiatta ipek böcekleri ve örümceklerin vücut salgısı olarak üretilen fibroin, gelişen rekombinant DNA uygulamaları sayesinde laboratuvar ortamında mikro-organizmalar tarafından da üretilebilir hale gelmiştir. Bilhassa bu materyalin canlı organizmalarla mükemmel biyouyumluluğu, fibroini en gözde biyomalzemelerden biri haline getirmiş ve doku mühendisliği, kontrollü ilaç salınımı gibi uygulamalar için çok cazip bir alternatif kılmıştır.

Polimerik jeller, özünde çapraz bağlı polimer yapıda yumuşak ve ıslak malzemelerdir. Konvansyionel çapraz bağlı polimer termosetlerden farklı olarak jeller, polimerin çözünebildiği bir çözücü içerisinde çapraz bağlanır, böylelikle zincirler arası polimer bulunmayan çözücü ile dolu bölgeler muhafaza edilir. Bu gözenekli morfolojileri polimerik jellere katalizörler, süperkapasitörler, biyosensörler ve akıllı malzemeler gibi pek çok kullanım alanı yaratmıştır. Sıklıkla kullanılan çözücü tipine bağlı olarak sınıflandırılan jeller temel olarak, hidrojel, organojel ve aerojel olarak üç sınıfa ayrılırlar. Bu tip jellerde sırasıyla su ve organik çözücüler çözücü olarak kullanılırken, aerojellerde ise çözücü süperkritik kurutma yahut solvent değişimi ile yerini havaya bırakır. Hidrojeller, yapılarında %90'ın üzerinde su ihtiva ettiklerinden canlı hücreler ve dokularla büyük oranda uyum gösteren yapılardır.

Kriyojel, özel bir hidrojel sınıfıdır. Konvansiyonel hidrojeller termal radikalik başlatıcı vasıtasıyla 0 ^{o}C'nin üstündeki sıcaklıklarda üretilirken kriyojeller, çeşitli başlatıcı yahut katalizörler yardımıyla 0 ^{o}C'nin altındaki sıcaklıklarda, bir başka ifadeyle 'kriyojenik şartlarda' sentezlenirler. Burada jelleşme reaksiyonu için gereken etki, yüksek sıcaklıklardaki aktivasyon enerjisinden değil, donmuş solvent içerisinde donmadan kalan yüksek konsantrasyon bölgelerinde jel bileşenlerinin derişiminin artması ve sıkışmasından ileri gelir. Bu duruma 'kriyo-konsantrasyon etkisi' denir. Bu etki, kriyojellere daha muntazam bir gözenek morfolojisi kazandırır ve çeper kalınlığı dağılımı sağlar. Bu düzgün gözenekli yapı kriyojellere, hidrojellere nazaran daha hızlı şişebilme, uyarıcılara daha çabuk tepki verebilme, daha üstün mekanik özellikler ve parçalanmaksızın birkaç kez sıkıştırılıp yeniden şişebilme gibi üstün özellikler kazandırır. Ayrıca polimerik kriyojellerin, elektron mikroskop görüntüleri incelendiğinde, hücresizleştirilmiş insan ekstraselüler matrisine gösterdiği kayda değer bir benzerlik kolaylıkla fark edilebilmektedir. Tüm bu özellikleri, polimerik kriyojelleri doku mühendisliği uygulamaları açısından oldukça kıymetli malzemeler haline getirmiştir.

Polimerik jellerde konvansiyonel kovalent çapraz bağlar yer alabileceği gibi, bu bağların yanı sıra ya da yalnızca kovalent olmayan çapraz bağlanmalar da bulunabilir.

Bu çapraz bağlanmalar, moleküller arası ikincil etkileşimlerden (hidrojen bağı, iyon-dipol, Van der Waals vs.) ileri gelen elektrostatik etkileşimlerdir. Normalde iyonik yahut kovalent etkileşimlere nazaran çok zayıf kabul edilen bu kuvvetler, sayıları ve yoğunlukları molekül boyunca çok arttırıldığında molekül konformasyonunu sabitleyecek kadar güçlü bir etki yaratabilirler. Bu bağların güçlü etkileşimlerin aksine dış uyaranlar vasıtasıyla (UV, ısı, elektrik, özel iyonlar ve moleküller) tersinir olarak kaybolup yeniden oluşabilme özellikleri, bu nevi bağlar içeren polimerik jellere akıllı malzeme özellikleri kazandıran temel prensiptir. Bağları dağıtan etkilere 'uyarıcı' (stimulus); bu etkilerle özellikleri değişen malzemelere de 'uyarıcılara duyarlı' (stimuli-responsive) malzemeler denir. Bu 'akıllı malzemeler', uyaranlar karşısında hacim, şekil, mekanik mukavemet, elektrik iletkenliği gibi çeşitli özelliklerini değiştirebilme yetisine sahiptirler. Özellik değiştiren bu akıllı malzemeler kontrollü ilaç salınımından yumuşak robotiğe, biyosensörlerden aktüatörlere geniş çapta uygulama alanına sahiptirler.

Bu tez çalışması kapsamında, *Bombyx mori* türü ipek böceği kozasından izole edilen ipek fibroin proteininden mamul kriyojeller, donmalı kurutucu ile kurutulmaları sonrası gözeneklerin içinde hidrofobik *n*-oktadesil akrilat (C18A) ile aksrilik asit (AAc) kopolimeri bir organojel termal polimerizasyon ile oluşturularak ipek fibroin kriyojellere şekil hafıza özelliği kazandırılması amaçlanmıştır. Bu yeni bifazik yapı, polimerik kriyojel bazlı organohidrojel (OHG) olarak nitelendirilmiştir. OHG'ler, konvansiyonel jellerin aksine yapılarında hidrofilik ve oleofilik segmentler bulundururlar. Tabiattan ilham alan OHG'lerin sentezlenmesinden amaç, çeşitli canlıların vücutlarında görülen bu tür yapıların canlılara verdikleri ekstrem koşullara dayanım ve ayarlanabilir mekanik özellikleri gibi akıllı malzeme özelliklerini sentetik olarak taklit etmede bir yaklaşım geliştirmektir. Ayrıca bu malzemeler, şekil hafıza özellikleri münasebetiyle yumuşak robotik gibi uygulamalarda ümit vaat eden alternatiflerdir.

Mikro-organojel ağın OHG özelliklerine etkisi iki seri malzeme geliştirilerek araştırılmıştır. İlk grup malzemeler sabit ipek fibroin başlangıç konsantrasyonunda (%5 ağ/hac) kriyojellere, farklı C18A mol kesrinde (%10-30) organojeller yüklenerek dört farklı OHG oluşturulmuş, ikinci grup malzemeler ise farklı ipek fibroin konsantrasyonlarında kriyojellere (%5-20 ağ/hac) sabit C18A mol kesrinde (%30) organojeller yüklenerek bu defa fibroin konsantrasyonunun yapısal özelliklere etkisi irdelenmiştir.

Başlangıçta farklı fibroin konsantrasyonlarında üretilen kryiojeller, saf suda şişme özellikleri, gözenek morfolojisi ve boyutları, tek eksenli sıkıştırma testleri ile mekanik özellikleri bakımından, kuru ve ıslak durumda karakterize edilmiştir. Kriyojel gözenekliliğinin %5'ten %20'ye artan fibroin konsantrasyonu ile %92'den %74 seviyesine azaldığı ölçülmüştür. Taramalı elektron mikroskobu (SEM) görüntülemesi ortalama gözenek çaplarının 25,7 μm'den 16,8 μm'ye azaldığını göstermektedir. Fourier-Dönüşümlü Kızılötesi Spektrometrisi (FTIR) ölçümleri, artan fibroin konsantrasyonu ile *β*-tabaka düzeyinde %10 artış olduğunu ortaya koymaktadır.

Donmalı kurutucu ve organojel sentezi sonrası OHG gözenekliliğinin %45-8 aralığına azaldığı görülmüştür, kriyojeller için hesaplanan 17,3 – 2,9 mL/g aralığında olan gözenek hacmi değerleri, OHG'ler için 0.16 mL/g seviyesine dek azalmıştır. Kriyojeller için en az 0,04 MPa düzeyinde olan Young Modülü değerinin, artan fibroin konsantrasyonu ve C18A mol kesri ile 17,7 MPa'a kadar yükseldiği görülmüştür.

OHG haline gelen kriyojellerde kopma gerinimi yüzde on azalırken, kopma geriliminin on kat kadar arttığı gözlenmiştir.

OHG'lere akıllı malzeme yetilerini kazandıran özellik, organojel ağ yapısına katılan C18A monomerlerinin uzun hidrokarbon zinciri yapısındaki kuyruklarının kümelenerek kristallenmesine yol açan hidrofobik etkileşimlerdir. OHG içerisinde oluşturulan birbirine bağlı mikro-organojel yapının sıcaklığa bağlı özellik değişimleri diferansiyel taramalı kalorimetri (DSC) ve reometre testleri ile gözlemlenmiştir.

İlk seride artan C18A mol kesrinin yapıdaki ikincil etkileşim miktarını arttırdığı gözlenmiştir. Bu etki, DSC eğrilerinde erime ve kristallenme pik alanlarındaki artıştan hesaplanan kristalinite indeksi (f_{cry}) adı verilen bir parametre üzerinden mukayeseli olarak ortaya konmuştur. Bu değer, organojel içerisinde kristalin yapıya katılan C18A monomerlerinin fraksiyonunu ifade etmektedir. Malzemeler 0 – 80 ^{o}C sıcaklıklar arasında iki döngü halinde ısıtılıp soğutulduklarında, DSC eğrilerinde poli(*n*-oktadesil akrilat) hidrofobik kristallerinin erime ve kristallenmesine atfedilen pikler sırasıyla ısıtmada 54 ^{o}C ve soğutmada 43 ^{o}C dolaylarında gözlenmiştir. Erime entalpileri gözetilerek hesaplanan f_{cry} değerleri C18A mol kesri %30'dan %10'a azaldığında, %15,7 ± 0,01'den %2 ± 0,3'e azalmıştır. Yapılan bükme şekil hafızası testleri neticesinde ise C18A mol kesri en yüksek olan (%30) OHG'lerin verilen kalıcı şekilleri tam bir başarıyla tutabilirken, en düşük mol kesrine sahip (%10) OHG'lerin verilen geçici şekli tam olarak sabitlemeyemedikleri gözlemlenmiştir.

İkinci seride ise artan fibroin konsantrasyonunun gözenek boyutunu küçültmesi ve kriyojel çeper kalınlığını arttırması sonucu mikro-organojel yapıda ikincil etkileşimlerin daha az miktarda oluştuğu ortaya çıkmıştır. Hesaplanan f_{cry} değerlerinin, %5'ten %20 ağ/hac'ye artan fibroin konsantrasyonları ile %15,7 ± 0.01'den %2,9 ± 0,08'e düştüğü gözlemlenmiştir.

X-Işını Kırınım (XRD) testleri ile kriyojel ve OHG'lerin morfolojisi derinlemesine araştırılmıştır. Kriyojellerde artan fibroin konsantrasyonu ile 2θ = 9,5 ^{o}, 20 ^{o}, 24.6^{o} açılarına karşılık gelen piklerin büyüyüp keskinleşmesi β-tabakalar gibi düzenli formasyonların artışını ortaya koymuştur. OHG'lerin XRD desenlerinde ise, kriyojellerde görülmeyen ve d = 0.41 nm aralığına tekabül eden 2θ = 21.6^{o} pikleri, yapıda C18A kristalitlerinin oluştuğunu ortaya koymuştur. Artan fibroin konsantrasyonu ile bu piklerin küçülmesinin, daralan gözeneklerde kristalin bölgelerin oluşması için gerekli yönlenmenin gerçekleşmesinin zorlaşmasından ileri geldiği düşünülmektedir.

Oda sıcaklığında yapılan reometre ölçümleri neticesinde fibroin konsantrasyonu %5 ve C18A mol fraksiyonu %30 olan OHG'lerin, başlangıçta 1,5 MPa civarı olan elastik modülleri (G') 65 ^{o}C'a ısıtılmaları sonrası 220 kPa seviyesine düştüğü görülmüştür. Buna ek olarak malzemelerin tan δ değerlerinin frekansa duyarlı olarak değişimi de bu sıcaklıkta malzemelerin yumuşadığına dalalet etmektedir. OHG'ler yeniden oda sıcaklığına soğutulduklarında ise G' değerlerinin eski büyüklüğüne ulaştığı görülmüştür, bu da malzemede tersinir olarak eriyip kristallenebilen yapıların varlığının bir başka göstergesidir. Ayrıca yapılan şekil hafıza testlerinde üretilen tüm OHG'lerin, %95'in üzerinde şekil geri kazanım değeriyle şekil hafıza yeteneği sergilediği gözlemlenmiştir.

1. INTRODUCTION

Due to their hygroscopic nature, viscoelastic properties and biocompatibility [1–5], conventional hydrogels drew significant attention in the last decade. With the advancements in the research, some physical crosslinks which can reversibly be dissipated and regathered associated to the structure of the hydrogels along with permanent covalent crosslinks and that provided the hydrogels with adjustable physicochemical properties with the influence of external effects like pH [6], heat [7], light [8], electricity [9]. Thus, hydrogels with self-healing [10], shape memory [11], [12], multiple stimuli-responsiveness [13], [14] and self-adhesiveness [15] functionalities were produced. However, their soft and brittle network structure, mono-functionality and lack of the capability of adaptation to the environmental circumstances restricts the hydrogels' advanced technological applications. Although the improvement of mechanical performances of hydrogels was achieved through several strategies like nanocomposite hydrogels [16,17] and multiple-network hydrogels [18,19], these strategies still remained incapable of eliminating some problems stemming from the dispersive media being pure water, like freezing under subzero temperatures and losing their initial flexible and tough mechanical character of hydrogel [20] and lack of surface wettability adaptation once the environment of the hydrogel is changed [21].

Researchers who wanted to overcome these drawbacks for advanced applications headed to the examples in nature and they discovered a situation which they called "the binary cooperative complementary phenomenon" [22,23]. This phenomenon states that most of the time, the living organisms comprise of hydrophilic along with oleophilic physicochemical structures co-existing and cooperating simultaneously. With the aid of these hierarchical amphiphilic hetero-structures, for example, ectotherms and plants living in the polar regions can avoid freezing [24,25], molluscs like trepang can adjust their body stiffness and preserve from sea predators [26,27] and human skeletal muscle tissue exhibits superior mechanical endurance and advanced

controlled shape-changing ability [28,29]. Based on these examples, hetero-network "organohydrogels" (OHG), which are promising candidates for applications like freeze-tolerant [30], shape-memory materials [31], soft actuators [32] and adjustable surfaces [33] were developed.

There are four principle approaches to the OHG production. The first one is macroscopic organohydrogels strategy which comprise of a hydrogel and an organogel priorly synthesized and integrated by their interface in the macro scale [34,35]. The second one is the binary solvent OHG strategy which relies on the principle of conducting the *in-situ* gelation inside of a binary solvent (water-organic) system and changing the solvent following the gelation reaction [36,37]. And the third approach is the emulsion-based OHG strategy, in which one phase is dispersed in the other with the aid of amphiphilic copolymer or surfactant molecules to form an emulsion system and conduct the gelation reaction within [38]. Most of the time, the first network that comprises the continuous phase of the gel is conventional hydrogel thus it does not satisfy the necessary mechanical performance needed for most of the applications [39]. Besides, in general, the scopes of these strategies are mainly developing OHGs with freeze-tolerance, adjustable surface properties, non-swelling OHGs or OHGs with underwater adhesion properties.

In the scope of this thesis, a fast, simple and effective production method was developed based on the fourth OHG synthesis method, which is hetero-network OHG approach. An ethanolic organogel precursor was filled inside of the previously freeze-dried macroporous cryogels' μm sized pores and the thermal radicallic polymerization of organogels was conducted within these pores in order to produce OHGs. The procedure is visualized in Figure 1.1.

Unlike conventional hydrogel synthesis methods, in the cryogelation procedure which takes place under cryotropic conditions (below the freezing point of the solvent), cryogels that are mechanically robust, compressible up to high ratios without breaking, and with high swelling-deswelling kinetics can be produced [40].

Cryogels can preserve their stable porous structure and pore wall integrity when the water filled to their pores is removed by freeze-drying [41]. This feature makes

cryogels formidable candidates for this kind of OHG synthesis approach following the drying of the continuous first network.

In this regard, with the aim of OHG synthesis out of cryogel first networks, silk fibroin protein (SF) was first subjected to the gelation reaction at -18 ^{o}C and SF cryogels were produced. At that point in order to observe the influence of initial SF concentration on the cryogel porosity and thus, the organogel intake capability of cryogel, cryogels with 5, 10, 15, and 20 w/v % SF concentrations were synthesized. Later, the water filled to the pores of the produced cryogels was removed with freeze-drying and a macroporous SF network was procured.

This dry scaffold's pores were filled with ethanolic phase that contains organogel compounds of hydrophilic (AAc) and hydrophobic (C18A) comonomers, crosslinker and free radical initiator, then held at 50 ^{o}C for a day to conduct thermal polymerization. Hereby, a hetero-double network SF cryogel-based OHGs which contain micro-organogel coating within its macropores were achieved.

The adjustable mechanical and viscoelastic features of OHGs are achieved through reversibly dissociating and reforming hydrophobic interactions between the hydrophobic tales of C18A comonomers. So in order to investigate the influence of C18A content on the smart material abilities of OHGs, four different C18A mole fraction organogels of 10, 20, 25 and 30 % were prepared.

We observed that the mechanical properties of OHGs are much superior compared to those of their cryogel and organogel components. Cryogel porosity decreased with the increasing SF concentration from 92 to 74%. The crystallinity fractions of OHGs decreased from 15.7 to 2.9% with the increasing amount SF of the cryogel first network. Also, the increment in the C18A mole fraction of the organogel second network caused to an increase in the crystallinity fraction from 2 to 15.7%. The mechanical properties of OHGs differed above and below the melting point of the C18A crystallites. All OHGs produced exhibited a shape memory behavior with around 97% shape recovery ratio each.

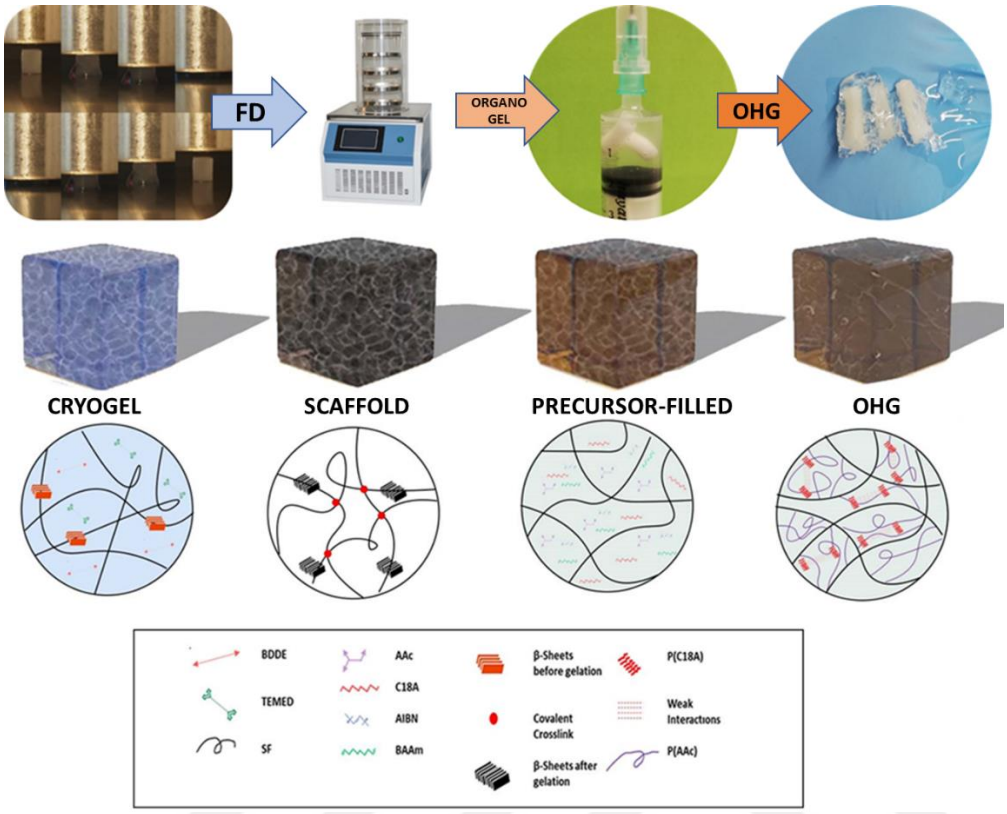

Figure 1.1: Schematic representation of OHG synthesis cosisting of four stages, namely, wet cryogel, freeze-dried scaffold, scaffold filled with organogel precursor, and OHG.

2. LITERATURE

2.1 Silk

Silk is a natural fiber produced by the epithelium cells of certain types of insects. It is a sticky and durable fiber that these insects use in order to protect their body during their metamorphosis procedure or to make their web out of it in order to catch their prey.

The commercial production of silk originated in China 5000 years ago and mankind first utilized silk fibers in textile production. Since then, silk is a common and popular material in the textile industry. Although there are many sorts of silk produced by various animals, domesticated *Bombyx mori* silkworm's cocoons are the most common resource of silk fibers [42]. With the recent advancements in technology, nowadays there are also recombinant silk proteins which are being produced *in vitro* by the activity of microbes [43].

There are also some other ancient usages of silk, like healthcare. Ancient Romans and Greeks were found to be using spider webs as wound dressing [44], and silkworm silk as surgical sutures [45]. Today, especially certain hierarchical proteins in the silk composition, like fibroin, draw great attention with their unparalleled properties for several biomedical applications.

2.1.1 Silk fibroin

The structure of silk is mainly comprised of fibroin and sericin polypeptides, along with other components like wax, carbohydrates, inorganic matter and pigments. In Table 2.1, the composition of the *Bombyx mori* silkworm is shown [46].

Sericin, the so-called 'silk gum' is the gummy protein that surrounds and holds the fibroin fibers together. Sericin can be eliminated by the 'degumming' process, which

denotes the boiling of silkworm cocoons in the alkali solutions [47]. In the end, a wool of SF is handed as seen in Figure 2.1.

Table 2.1: Percent composition of the structural elements in silk fiber.

Component	%
Fibroin	70-80
Sericin	20-30
Wax	0.4-0.8
Inorganic matter	1.2-1.6
Pigments	0.7
Total	100

Figure 2.1: Bombyx mori silkworm, its cocoon and the fibroin wool derived out of the cocoon.

Silk fibroin protein is a polypeptide that mainly drew attention due to its significant mechanical properties like extraordinary tensile strength. The majority of the amino acids that are present in the fibroin structure are glycine (Gly) (43%), alanine (Ala) (30%) and serine (Ser) (12%) [47]. This strength arises from the secondary interactions comprised of the H-bonds and van der Waals interactions. These bonds are due to the

repetitive glycine-alanine-glycine-alanine-glycine-serine (GAGAGS) amino-acid sequences (Figure 2.2) in the fibroin structure [48]. These sequences are glycine-rich amino acid sequences, which is a hydrophobic amino acid capable of creating weak intra and inter-molecular interactions. The reason these blocks exhibit such strong crystallization ability is due to the cooperation of hydrogen side chains of glycine and methyl side chains of alanine populating the hydrophobic domains. These domains create the regulated secondary structures called β-sheets (Figure 2.3).

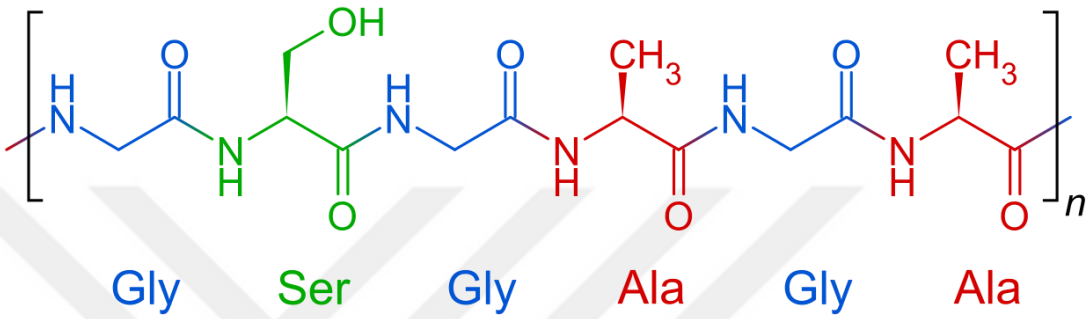

Figure 2.2: Chemical structure of the silk fibroin repeating units with alaine, glycine and serine indicated in red, blue and green, respectively.

2.1.2 Structural orders of silk fibroin and fibroin gelation

There are 4 main structural orders in silk fibroin proteins. The primary structure of SF defines the molecular chains that are comprised of amino acids and peptide bonds between them. The secondary structure of fibroin is regulated by the inter-molecular weak interactions' cooperative acts. Examples of secondary interactions are α-helixes, β-sheets, and random coils Figure 2.3. The tertiary structures are formed by the secondary interactions folding over each other in 3-dimensions. The quaternary structures are combinations of tertiary structures and they are only observed when the protein comprises of multiple polypeptide chains.

The secondary structures of α-helixes and β-sheets differ in terms of the organization of the molecules. α-helixes are intra-molecular formations, whereas β-sheets are intermolecular compositions that are formed by multiple folded ladder sheets that fold over each other. These β-sheet structures significantly intensify the mechanical properties of silk with an increased ratio of these conformations to the overall fibroin structure [49]. In general, these β-sheet and β-turn formations provide the fibroin with

strength and durability, and the other less ordered formations like α-helixes and random coils (hydrophilic blocks) provide elasticity and toughness to the material.In general, these β-sheet and β-turn formations provide the fibroin with strength and durability, and the other less ordered formations like α-helixes and random coils (hydrophilic blocks) provide elasticity and toughness to the material.

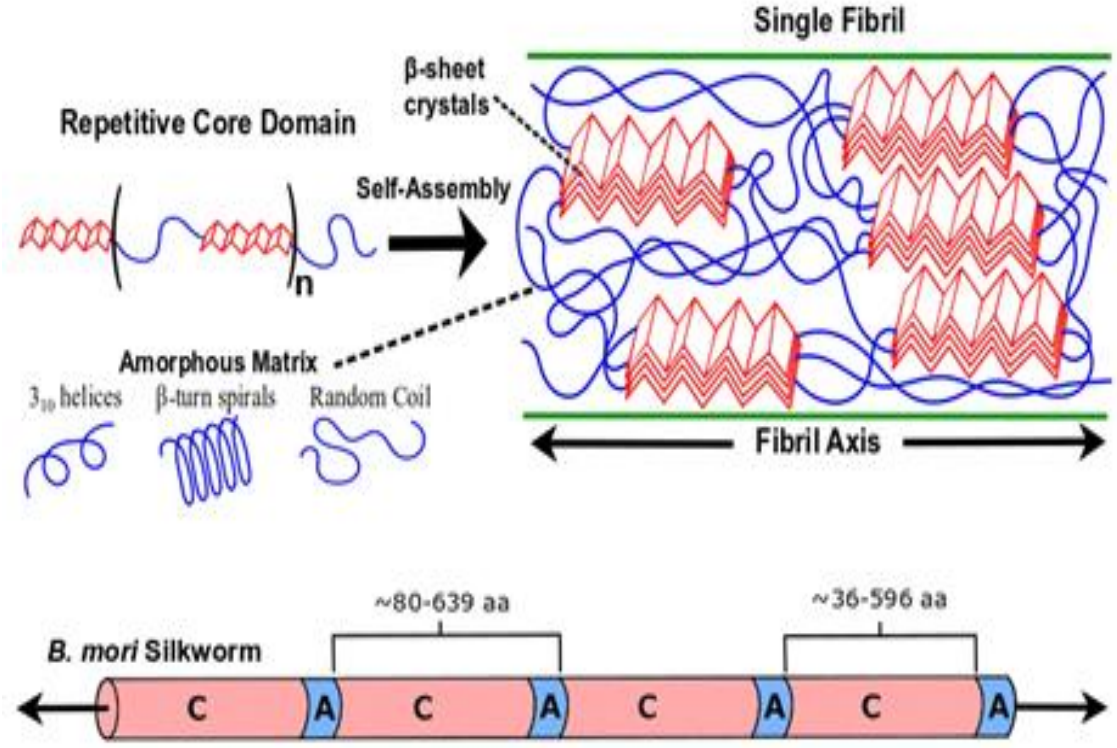

Figure 2.3: Crystalline and amorphous conformation types within a single fibroin fiber and altering crystalline (C) – amorphous (A) chain segments distributions of *Bombyx mori* silkworm's silk. Crystalline segments are rich in glycine hydrophobic amino acids. Arranged with permission from Ref. [50]

Although various forms of SF-based materials are investigated as valuable biomaterials such as mats, films, sponges and hydrogels [47], SF hydrogels gained significant attention among them with their structure and abilities that make them formidable materials for bio-applications such as drug delivery and tissue engineering [51]. The gelation of SF, which is illustrated in Figure 2.4, mainly happens with the influence of these β-sheet secondary structures [52]. This gelation procedure takes more time than other common proteins' gelations and is affected by many parameters

like pH, temperature, and concentration. For instance, with increasing pH of the reaction environment, the gelation reactions of SF occur slower, due to the osmotic pressure of carboxyl groups attached to SF main chains getting ionized at high pH value. In an aqueous reaction environment, with the facts that keep SF chains surrounded by water molecules, like this counter-ion caused swelling and dilution, SF gelation takes longer to conclude. Because water prevents the SF chains from folding over each other and β-sheets cannot form hydrophobic secondary interactions between them.

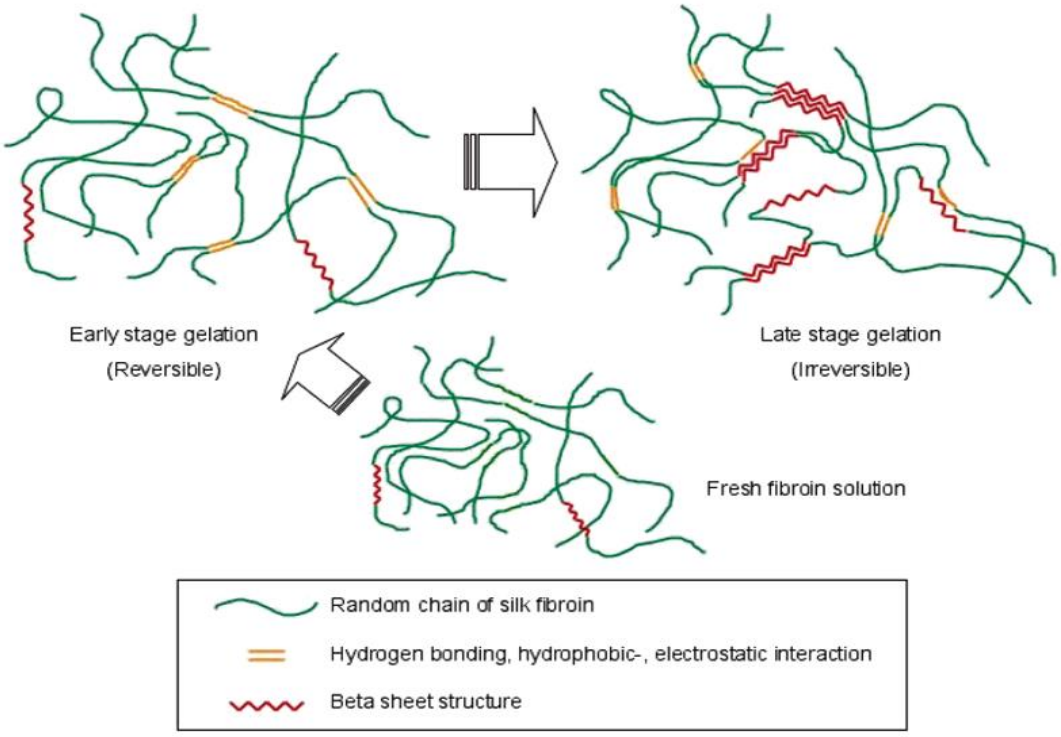

Figure 2.4: Conformation and assembly of silk fibroin (SF) molecular chains at fresh solution, early state gelation and late state gelation situations. Reprinted with permission from Ref. [52].

At an acidic pH region, however, it is easy for SF chains to create hydrophobic intermolecular interactions because the ionization of the carboxyl groups attached to SF is restricted and this hinders SF's expansion capability in water. Colliding SF chains trigger gelation reactions with more efficient β-sheets formations between hydrophobic domains [53]. However, it might still take SF to become gel at a 3% concentration for two days [54]. An approach by our research group to accelerate this reaction was treating the SF with diepoxide crosslinkers [55]. Specifically, the

ethylene glycol diglycidyl ether (EGDE) and 1,4- butanediol diglycidyl ether (BDDE), which are commonly used diepoxide resources for crosslinking of various natural macromolecules were used in that manner [41]. This method is valid to shorten the gelation period because epoxide groups of BDDE interact with the amine side groups of hydrophilic regions of two different SF chains and reduce chain mobility. Thus, the interactions between SF molecules grow stronger and they form β-sheets faster.

2.2 Polymeric Gels

Gels are defined as the intermediate matter form between solid and liquid [56]. That is because gels comprise two components: a solid (polymer) and a liquid (solvent). The difference of gels from polymer solutions is the crosslinks that are keeping the molecular chains of gels together and restrict them from getting dissolved. The polymer network restrains the liquid within from flowing away and the solvent phase prevents the polymer chains to collapse and cluster. That is why gels possess different viscoelastic behavior from conventional pure solid polymers. Also, intermolecular covalent crosslinks make gels a single, macroscale molecule whose molecular weight is accepted to be infinite. So the conformational changes in the molecular chain segments of gels result in visible changes in the macroscale properties of the gels. The figure below Figure 2.5 shows the structure of the covalently crosslinked gels in a general manner. At the macro-scale, they are seen as water-filled monoliths which are generally transparent or blurry.

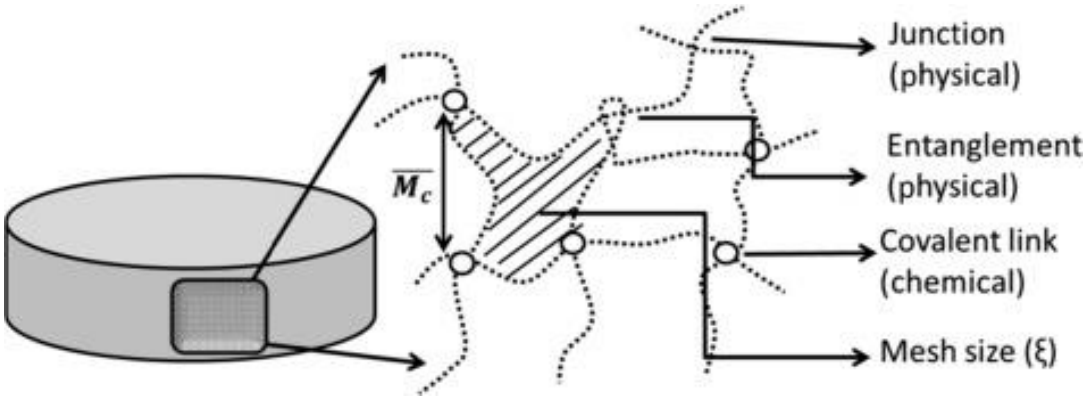

Figure 2.5: Schematic representation of polymeric gels. Taken from Ref. [57] with permission.

At the micro-scale, they consist of molecular chains (dotted lines), physical junctions, topological entanglements, and covalent crosslinks (hollow circles). All the gaps between polymer chains, the so-called pores of the gels are occupied by solvent molecules.

2.2.1 Hydrogels

Hydrogels are polymeric gels formed by crosslinking of hydrophilic polymer chains in an aqueous media [58]. Their pores separated by water give them the ability to undergo reversible phase transitions, especially with certain effects like pH, temperature, light, magnetic field or chemical agents [59]. These sorts of so-called 'stimuli-responsive' hydrogels are investigated for a broad range of applications, especially in the biomedical field due to the hydrogels' bio-mimetic architecture, and hydrophilicity, having necessary spaces within their structures for cell viability and conduction of nutrients, etc.

Although hydrogels became so popular due to these features of them, they have also certain handicaps that restrict them from practical applications, such as lack of rapid phase transition and mechanical robustness. To enhance the toughness and strength, thus the applicability of hydrogels,

The rapid phase transition is required for the applications for which a fast stimuli response rate is required. The main concern of the efforts in order to give the hydrogels faster stimuli response rates is arranging their diffusion properties and swelling kinetics. There are several strategies applied for that purpose like reducing the gel particle size [60,61], attaching dangling side chains with one end attached to the gel, the other is free [62] and developing a macroporous gels approach that relies on creating some sacrificial diluents within the continuous main network and then eliminating it [63].

2.2.2 Cryogels

Another novel approach to enhance hydrogels' porosity is creating solvent templates within gel precursor solution, under the freezing temperature of solvents. This method is called cryogelation [40]. In cryogelation, after the gel components are gathered in the gel precursor, the gelation reactions are conducted at subzero temperatures. When

the solvent phase gets frozen at that temperature, gel components are accumulated in the unfrozen high concentration channels with the influence of the effect called ‘cryoconcentration’ [64]. Once the cryogels are synthesized and then thawed, frozen solvent domains in the cryogel network form interconnected, μm-sized water-filled domains, e.g., so-called ‘macropores’. The cryogelation process is illustrated in Figure 2.6.

Although polymeric hydrogels are thoroughly investigated for biomedical purposes, their pore size generally does not meet the requirements of such applications, they possess rather limited mechanical performance and their diffusivity for oxygen and nutrients are also limited [65].

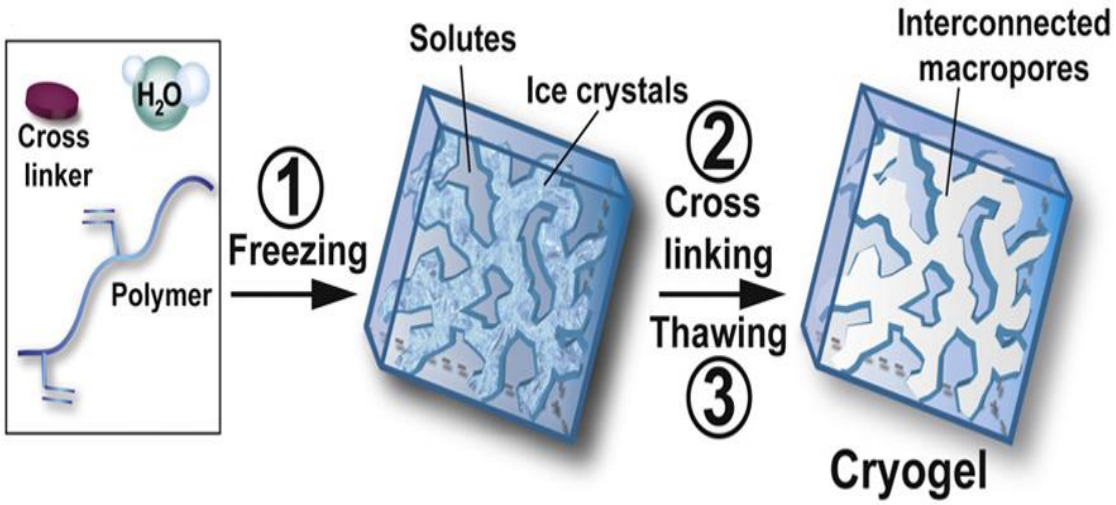

Figure 2.6: Schematic representation of cryogelation procedure. Pregel components, frozen gelation system and thawed macroporous cryogels. Adapted from Ref. [65] with permission.

The reason behind this is the weak and unsteady structure of the hydrogels. Due to their relatively thicker and stronger pore walls, and interconnected macropores with homogenous pore size distribution [41], cryogels meet the requirements of biomedical applications better than conventional hydrogels [65]. Also, their macroporous structure and ability to withstand repetitive cyclic deformations [66] are enabled cryogels for various other applications like superadsorbents [67,68], catalysts [69,70], and separation membranes [71,72].

2.3 Shape Memory Polymers

Ability of natural materials and biological organisms to adjust their properties upon external influences have inspired materials scientists to design novel materials which exhibit such behaviour [73].

For instance, sea cucumbers adjust their body stiffness to get protected from predators [74], and chameleons change their body color to blend in the environment and hide in plain sight in seconds [75]. Scientists have deep-dived into such occurring in nature and discovered that these sorts of 'stimuli-responses' are all influenced by molecular-level changes. Figure 2.7 shows the various types of shape memory polymers and their dimensional responses against externat stimuli.

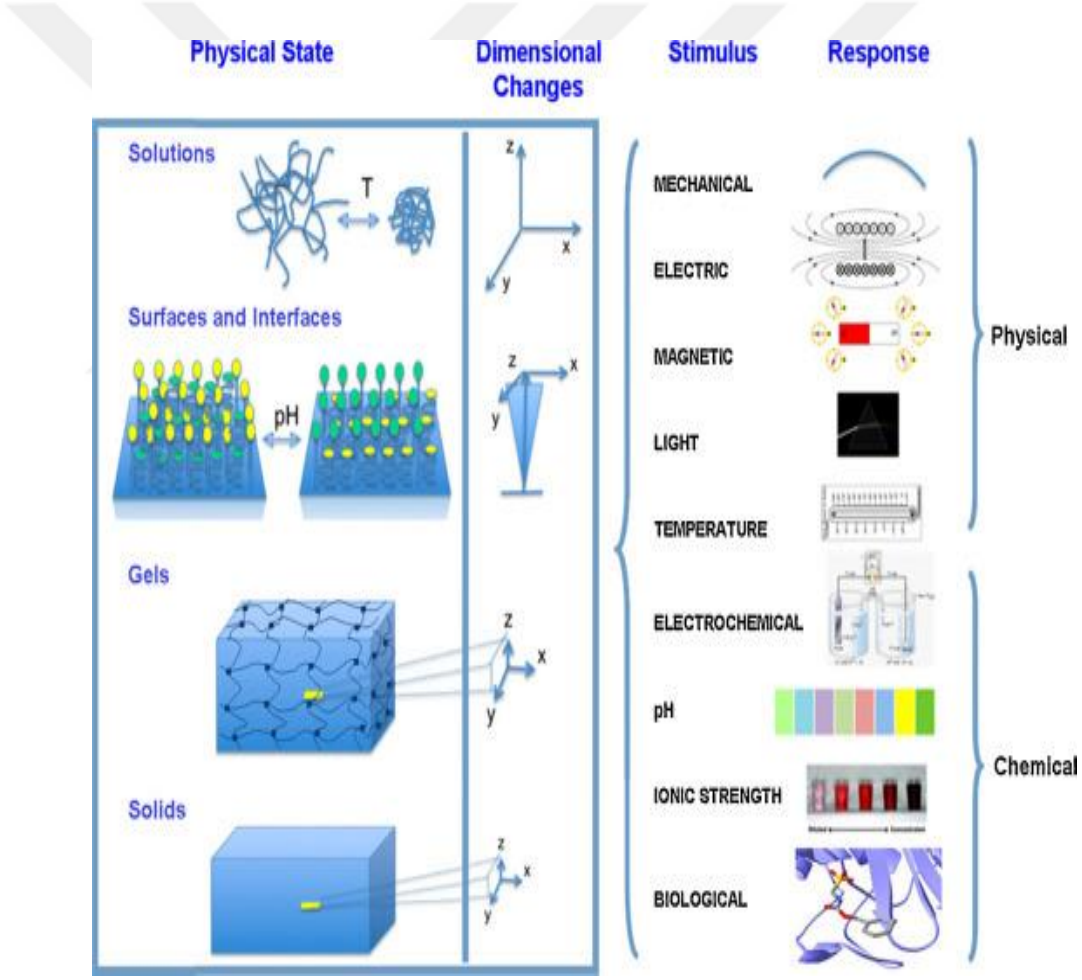

Figure 2.7: Shape memory polymers in various material forms, and their dimensional changes in response to various external stimuli. Directly taken from Ref. [78] with permission.

One of the types of these varied stimuli responses is the shape memory ability of polymers. Shape memory polymers respond to some external stimuli (generally heat) and transform from a temporary shape programmed on them to a permanent shape they 'memorized' [76]. This is generally due to the release of temporary intermolecular interactions established within the structure, and molecular chains of the polymer turn back to their original conformation due to the conformational elasticity [77].

Even though the first known report on such 'shape memory' polymers was a patent of a dental implant resin, they have gained greater attention with the development of heat shrinkable tubing and films out of covalently crosslinked polyethylene [76].

2.3.1 Shape memory hydrogels

Shape memory ability stems from the biphasic organizations of polymers: a constituted network as a permanent scaffold and an additional reversibly forming and disappearing phase [76]. The first network, which generally constitutes permanent covalent crosslinks, takes on the 'memorizing' function and recovers back to the permanent shape once the stimulus is applied, and the second phase is reversibly formed and disappeared for the purpose of fixing the temporary shape of the material. In gels, this effect is generally situated by creating the opposite nature interactions within a hydrogel, for instance adding alkyl side chains with the ability to form hydrophobic secondary interactions within an aqueous media.

The crystalline domains formed by these hydrophobic nanocrystallites reversibly disappear when the ambient temperature exceeded their melting temperature (T_m). At that stage, generally, an abrupt drop in the material's mechanical performance is observed due to the disappearence of additional crystalline formations, the material can be easily deformed.

Once this deformed temporary shape is cooled down to a temperature below T_m, the crystalline domains get reformed both enhancing the mechanical toughness of the material and fixing the temporary shape given to the material. This reversible melting and crystallizing are visualized in (Figure 2.8).

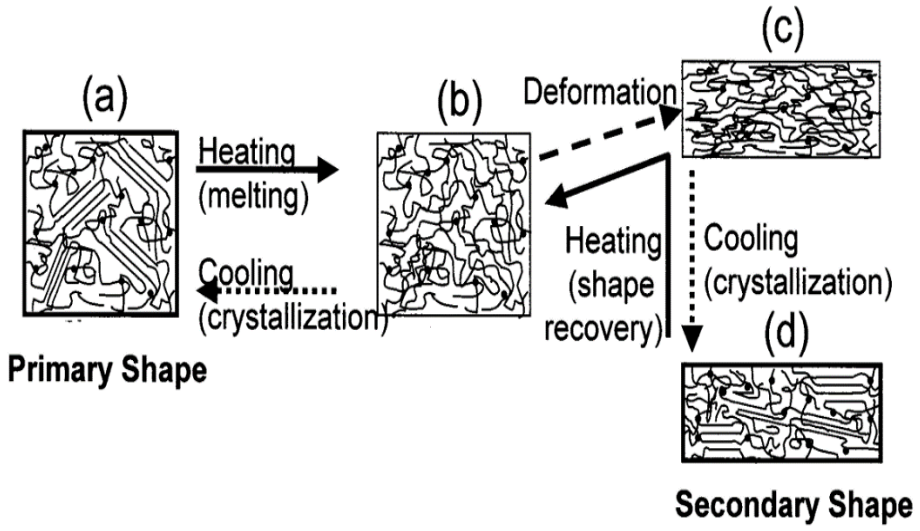

Figure 2.8: Schematic representation of weak interactions-induced shape memory principle in hydrogels. (a) Permanent primary shape, (b) heated material with melted crystalline domains, (c) deformed hot material and (d) temporary secondary shape fixed via cooling under deformation. Directly taken from Ref. [79] with permission.

By associating more than two phases in the gel structure together, it is possible to fix even more than one temporary shape. These gels are called multiple-shape memory hydrogels [80,81].

2.3.2 Bio-inspired, shape memory organohydrogels

Although the improvement of mechanical performances of hydrogels was achieved through several strategies like nanocomposite hydrogels [16,17] and multiple-network hydrogels [18,19], these hydrogel materials are still seen as incapable of preserving their mechanical properties like toughness and elasticity, at extreme conditions like subzero temperatures [20] and lack of surface wettability adaptation once the environment of the hydrogel is changed [21]. With inspiration from creatures like extremophiles, scientists adopted another nature-inspired strategy to overcome these drawbacks, called “the binary cooperative complementary phenomenon” [22,23]. This principle states that most of the time, natural biological organisms include a hierarchical binary structure of hydrophilic and oleophilic parts co-existing and co-operating. Hereby, they came up with a novel biphasic gel type called ‘organohydrogels’ (OHG).

In recent years, several strategies were deployed for OHG production [82]. For instance, Zhao et. al. developed a strategy that relies on the gel-gel interface contraction through functional groups on their interface and fabricated a 'macroscopic layered' OHG [83]. On one end of OHG, there is an organogel part and on the other end, there is a hydrogel part. These two individual parts are only chemically conjugated on their interface and each end preserved its chemical nature. The aim of this method is to tune the surface wettability of OHG in different media.

Another approach developed by Li et al. is called the site-specific "*in situ*" transformation strategy [84]. In this work, researchers treated specific chemical sites on poly(pentafluorophenyl acrylate) with aminolysis reactions to convert them into desired hydrogels, organogels, and even organo/hydro binary gels by coupling hydrophilic and oleophilic alkylamines on them. Scientists noted that the organo/hydro binary gels they produced via this method is promising for soft robotic applications due to the synergistic effect of organogel swelling and hydrogel shrinkage.

In another work inspired by mussel adhesion chemistry, Han et al. developed a cell adhesive, temperature and cold resistant and conductive OHGs for the purpose of bioelectronic applications [85]. In this system, a binary glycerol-water solvent system is deployed for the preparation of acrylic acid and acrylamide within the dispersed polydopamine-decorated carbon nanotubes solutions. Resulting from the vast hydrogen bonds between polyol and water, OHGs preserved their mechanical performance and conductivity even at subzero temperatures. The concern here is the inadequate long-term stability of low molecular weight alcohol-network interactions. Also, dissociated alcohol is predicted to probably weaken the OHGs mechanically after long durations.

Another very commonly applied method for OHG synthesis is emulsion-based OHGs [86–89]. In this method, the oleophilic discontinuous phase is dispersed in an aqueous continuous phase or otherwise, and the dispersed phase gets emulsified with the aid of dispersive mixing, surfactants or amphiphilic comonomers or is subjected to an *in situ* gelation within a continuous phase. Regarding to the density and the manner of the dispersed phase within OHG, the methods are classified into two: (a) entrapped dispersed phase droplets that does not intact with the main network and (b) dispersed

droplets are crosslinked into micro-networks that contribute to the main network. Zhao et al. utilized this method in order to prepare an OHG comprised of *N*,*N*-dimethylacryamide aqueous continuous phase with lauryl methacrylate hydrophobic monomer droplets emulsified within [31]. The resulting OHGs exhibited an extraordinary shape memory capability, along with non-swelling behavior and adjustable mechanical and viscoelastic properties.

In another work that takes on this principle, Zhuo et al. developed multiple shape memory OHGs by incorporating different types of *n*-alkanes within the emulsion system (Figure 2.9) [90]. Hydrophobic monomers with different melting points within the discontinuous emulsion droplets have given the material different shape fixing heat intervals, thus OHGs possessed different temporary shapes as well as different mechanical characteristics between these intervals.

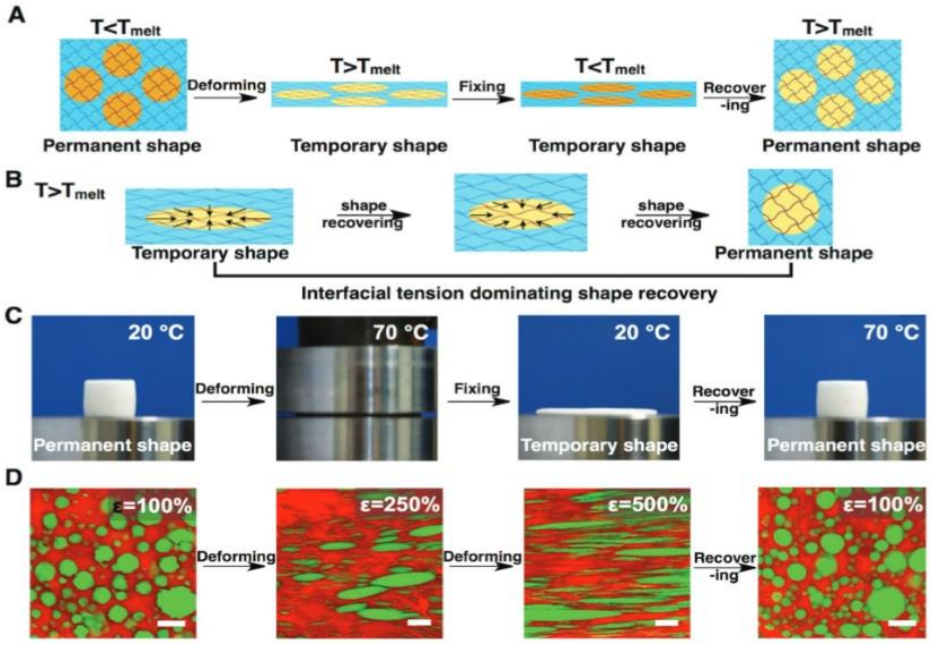

Figure 2.9: Schematic representations of (a) Shape memory and recovery of OHGs under tensile deformation, (b) shape memory and recovery of OHGs under compressive deformation. (c) OHG compressed into a flat temporary shape and heated for shape recovery. (d) Confocal laser scanning microscopy images of permanent, semi-compressed transitional, compressed and cooled temporary and recovered shapes of OHG. Red zone indicates the continuous hydrophilic network and green zones indicate emulsified oleophillic droplets. Directly taken from Ref. [31] with permission.

Another method for OHG synthesis is heteronetwork OHGs. In this method, a previously prepared hydrogel first network's water is eliminated via drying procedures, and after that dry hydrophilic network is filled up with oleophilic gel precursor, later reacted to form an ogranogel within the pores of first network (Figure 2.10). This method is very much like building multiple network hydrogels [19,91–94]. In contrary to ordinary multiple network gels, heteronetwork OHGs possess two or more [95] networks of distinctly different natures in terms of their hydrophilicity. For instance, in a recent work, Gao et al. used a preliminarily synthesized poly(*N*,*N*-dimethylacrylamide) hydrogel as a scaffold for organogel second network synthesis within [96]. A lauryl methacrylate and butyl methacrylate monomers-included ethanolic medium was filled into the acetone-dried hydrogel, and later subjected to *in situ* UV polymerization to synthesize the organogel second network. Ethanolic phase infused into the first network successfully due to its affinity to both heteronetwork monomers. The resulting heteronetwork OHG was seen successfully switching its surface configuration with changing media. Also, OHG exhibited a non-swelling behavior in either aqueous or organic medium. In another work of the same group, a hydrogel first network was consolidated with an oleophilic and an intermediate network [95]. Water and non-poler oil dispersion medium was utilized for synthesis procedure, later with the aid of acetone and dodecane, OHG swollen in oil was obtained and also water-swollen OHGs were prepared by immersing the as-prepared multinetwork OHGs directly into the water. The resulting OHGs exhibited a non-swelling behavior and adjustable surface configuration.

With reference to this approach, a novel synthesis method was recently developed by our research group [98]. In this procedure, the macropores of the cryogels based on methacrylated SF and poly(*N*,*N*-dimethylacrylamide) as a spacer were first filled with the precursor solution of organogel component. Free radical polymerization within the pores of the cryogels results in mechanically strong and temperature sensitive OHGs consisting of micro-organogel discontinuous and cryogel scaffold continuous phases with shape-memory function. The reason why cryogels are preferred instead of conventional hydrogels is due to the mechanical issues and cryogels' superior macroporosity as mentioned before.

In the present study, conventional SF cryogels of various initial SF concentrations (C_{SF}) were synthesized to be used as scaffolds for OHG synthesis. The main reason for changing the C_{SF} is to observe its influence on cryogel porosity. Cryogel scaffolds were filled with the ethanolic organogel precursor including acrylic acid (AAc) and n-octadecyl acrylate (C18A) monomers and subjected to free radical thermal polymerization. The resulting OHGs exhibited enhanced toughness and thermally adjustable mechanical and viscoelastic properties due to the hydrophobic interactions between C18A crystalline domains. In order to investigate the contribution of C18A amount to these properties, OHGs of four different C18A mole fractions with respect to the total monomers were synthesized. As will be seen below, silk fibroin based novel OHGs with a wide variety of mechanical properties and smart functions were prepared, which would expand their application areas.

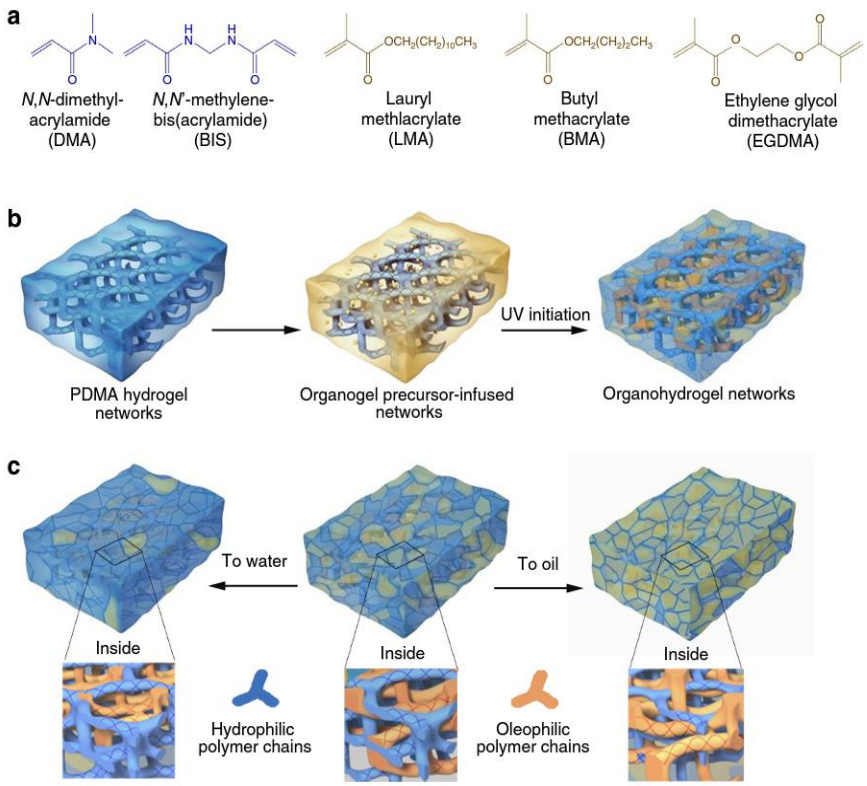

Figure 2.10: (a) Chemicals used for heteronetwork OHG synthesis. Hydrogel first network components indicated in blue, and organogel second network components are shown in yellow. (b) Synthesis steps of hydrogel, organogel precursor infused network and OHG. (c) Swelling behaviour of synthesized OHGs within aqueous and organic media. Hydrophillic first network is indicated in blue and oleophillic second network is indicated in orange. Directly taken from Ref. [97] with permission.

3. EXPERIMENTAL PART

3.1 Materials

Silk fibroin protein is naturally derived from the cocoons of *Bombyx mori* silkworms, provided by KozaBirlik in Bursa. Lithyum bromide (LiBr, molar mass 86.84 g/mol, Merck), sodium carbonate (Na_2CO_3, molar mass 105.99 g/mol Merck), 1,4-butanediol diglycidyl ether (BDDE, molar mass 202.25 g/mol, Sigma-Aldrich), *N*,*N*,*N*′,*N*′-tetramethylethylenediamine (TEMED, molar mass 116.24 g/mol, Sigma-Aldrich), n-octadecyl acrylate (C18A, molar mass 324.54 g/mol, Sigma-Aldrich, %97), *N,N'*-methylenebis(acrylamide) (BAAm, molar mass 154.17 g/mol, Sigma-Aldrich, %99), *α,α'*-azoisobutyronitrile (AIBN, molar mass 164.21 g/mol, Merck), ethanol (molar mass 46.07 g/mol, Merck, ≥ %99,9) and polyethylene glycol (PEG-10000, Sigma-Aldrich, molar mass 10000 g/mol) were used without purification. Acrylic acid (AAc, molar mass 105.99 g/mol, Merck) was purified from included hydroquinone inhibitor through a column filler separator. In Figure 3.1, the chemical structures of materials used for OHG production are given.

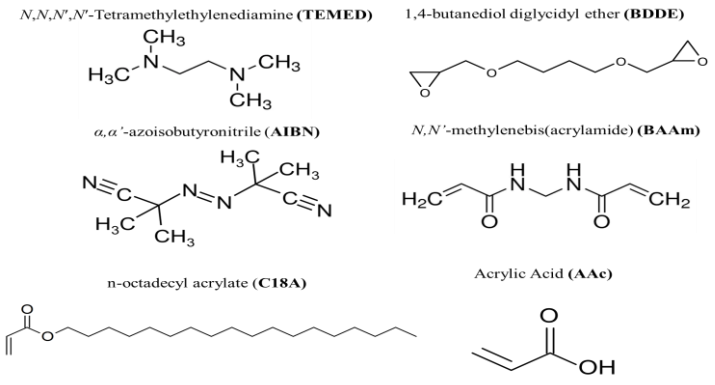

Figure 3.1: Chemical strucutres of the materials used for OHG synthesis*: N,N,N′,N′*-tetramethylethylenediamine (TEMED), 1,4-butanediol diglycidyl ether (BDDE), *α,α'*-azoisobutyronitrile (AIBN), *N,N'*-methylenebis(acrylamide) (BAAm) , n-octadecyl acrylate (C18A) and acrylic acid (AAc).

3.2 Silk Fibroin Isolation from *Bombyx mori* Silkworm Cocoon

Silk fibroin (SF) isolation is done with reference to the method that previously reported [41], [99]. Briefly, 10 g of *Bombyx mori* silkworm cocoon is trimmed into mm-sized pieces and purged from the biologic residue within, later boiled for 1 hour inside a 1 L 0.02 M Na_2CO_3 solution in order to remove the sericin. The fibroin wool seperated from other components of silk was washed in pure water at 70 ^oC for 5 times, 20 minutes each and dried at room temperature. Dried SF wool of 7 g, dissolved in parts within a 35 mL 9.3 M LiBr solution at 60 ^oC. SF dissolved in solution was dialyzed within dialysis tubing (10000 MWCO, Snake Skin, Pierce) against pure water for 4 days. The pure water was freshed three times a day during this period and the LiBr was completely removed. The resulting SF solution's concentration was determined by the gravimetric method, and it was dialyzed against PEG-10000 solution inside a 3500 MWCO (Snake Skin, Pierce) when higher concentrations were needed in order to eliminate a certain amount of water.

3.3 Synthesis of Cryogels and Organohydrogels

In the present work, to investigate the influence of SF cryogel porosity on organogel precursor intake capacity and C18A crystallizability, cryogels with 4 different initial SF concentration (C_{SF} = 5, 10, 15 and 20 w/v%) were produced. Previous works proved that with increasing C_{SF} of cryogel precursor, the average pore size and percent porosity of cryogels were decreased [41]. For the purpose of pH regulation, TEMED was used at a fixed amount, 0,025 v/v % with respect to the total reaction mixture volume. BDDE crosslinker concentration was varied between 20 and 3 $mmol.g^{-1}$ in order to prevent the undesired instant gelation at high SF concentrations. Cryogel precursors prepared in this way were held inside of a refrigerator at -18 ^oC for 24 hours in plastic syringes of 1 mL volume and cryogelation was conducted. After the synthesized cryogels were thawed at room temperature, they were taken out of the syringes and immersed in pure water. With the purpose of eliminating the unreacted components and TEMED residue, cryogels were kept in pure water for 3 days. At the end of this duration, cryogels reached to the swelling equilibrium were freeze-dried with a Christ Alpha 2-4 LD-plus freeze drier. The freeze-drying procedure was constituted of three steps: (1) freezing step: one day at -25 ^oC, atmospheric pressure,

(2) main drying step: one day -40 °C, 0.12 mbar pressure and (3) final drying step: one day at -60 °C, 0.011 mbar. After three days, the macroporous SF cryogel scaffolds were obtained.

For organohydrogel (OHG) synthesis, SF cryogel scaffolds formed at C_{SF} = 5, 10, 15 and 20 w/v% were immersed in the ethanolic organogel precursor solutions at 40 °C containing AAc, C18A, BAAm and AIBN. In order to investigate the effect of C18A on the crystallinity of OHGs, C18A mole fraction (x_{C18A}) in the monomer mixture was taken as 0.1, 0.2, 0.25 and 0.3 at a fixed total monomer concentration of 41 w/v% (with respect to the organogel precursor solution). AIBN and BAAm amounts were also kept constant at 1 mol% with respect to the monomers. Cryogel scaffolds that reached to the swelling equilibrium in the ethanolic organogel solutions within 10 minutes under mechanical stirring, they were placed into 10 mL plastic syringes along with remaining organogel precursor solutions. Syringes were kept in an oven at 50 °C for 24 hours and the free radical polymerization of AAc, C18A, and BAAm was conducted (Figure 3.2).

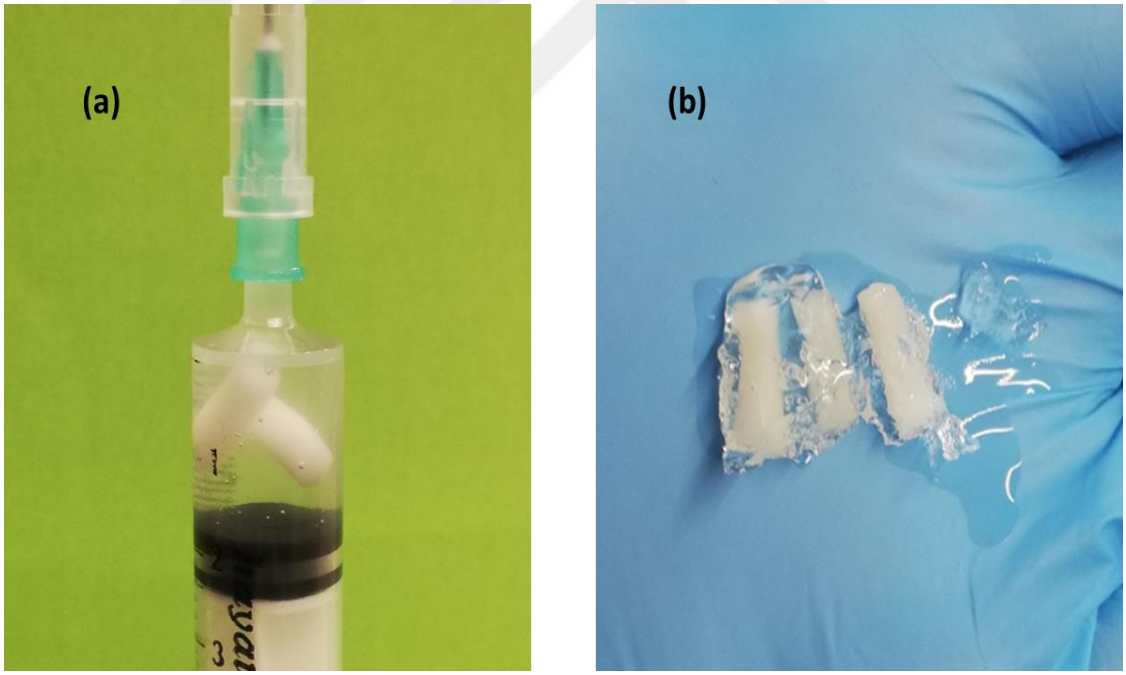

Figure 3.2: (a) Cylindrical cryogel scaffolds filled with organogel precursor are placed in a plastic syringe along with excessive precursor solution. (b) After free radical polymerization, OHGs are taken out of syringes and combed out of the surrounding excessive organogel.

Unreacted residues remaining in OHGs were eliminated after the OHGs produced were combed out of the surrounding excessive organogel layer and kept in ethanol for at least a week. In order to compare their mechanical performances with OHGs, poly(AAc-co-C18A) organogels whose C18A mole fraction are x_{C18A} = 0.3 were synthesized under the same conditions. For organogel synthesis, AAc (1.32 mL) and C18A (2.70 g) were initially dissolved in ethanol at 40 ºC, and once the solution was homogenized, BAAm and AIBN were included respectively and finally, the reaction mixture was topped with excess ethanol in order to complete the total reaction mixture amount to 10 mL. Organogel precursor gelation was carried out in an oven at 50 ºC for 24 hours within plastic syringes of 1 mL.

3.4 Characterization of Cryogels and Organohydrogels

3.4.1 Swelling tests of cryogels and organoohydrogels

The mass (q_w) and volume (q_v) swelling ratios of cryogels and OHGs were calculated according to the equations (3.1) and (3.2), respectively.

$$q_w = \frac{m}{m_{dry}} \tag{3.1}$$

$$q_v = \left(\frac{D}{D_{dry}}\right)^3 \tag{3.2}$$

Here, the symbols without subscripts *m* and *D* stands for the mass and diameter of the gels at swelling equilibrium, where m_{dry} and D_{dry} symbolizes the mass and diameter of the dry networks, respectively. The gel fraction (W_g), which defines the proportion of the gel components contributed to the crosslinked network strucutre, was calculated regarding to the equation (3.3).

$$W_g = \frac{m_{dry}}{(m_0 C)} \tag{3.3}$$

In this equation, m_0 defines the mass of the gels at as-prepared state. C is the total concentration of the reacted components.

To determine the porosities of cryogels and OHGs, their swelling ratios within water, q_w and q_v, were used. The reason for that is; q_v is the measure of the stretching of pore walls, where q_w incidcates the change in the solvent mass within the pores of the gel. The difference between these two values is due to the porous nature of the materials. Total porosity (P) was calculated regarding to the following equation (3.4) [100].

$$P = 1 - q_v[1 + (q_w - 1)\rho/d_1]^{-1} \tag{3.4}$$

The expressions d_1 and ρ in the equation refer to the density values of water (1 g.mL^{-1}), and SF (1.35 g.mL^{-1}) or OHG (1.1 g.mL^{-1}), respectively. To calculate the total volume of the pores (V_p), water with pH=3 was used, which interacts with neither the cryogel nor the OHG of the pore walls and does not cause swelling by volume.

It was observed that the gels immersed in water at pH = 3 did not show swelling in volume, while their mass significantly increases. This increase was attributed to the mass of water filling the pore volume. Based on this quantitative observation, V_p was calculated using equation (3.5).

$$V_p = {d_1}^{-1}(m/m_{dry} - 1) \tag{3.5}$$

3.4.2 Conformational analysis of cryogels and organohydrogles

Conformational analysis of SF cryogels was performed with the Agilent Technologies Cary 630 ATR-FTIR spectrophotometer as reported previously [66,99]. In summary, the outline of the Amide-I region of the spectrum was first arranged linearly and then deconvolved according to the Gaussian model in PeakFit (version 4.12, SeaSolve Software Inc.) software. After that, four curves corresponding to 1620, 1640, 1660,

and 1698 cm^{-1} band positions were fitted, corresponding to the β-sheet, random coil, α-helix, and β-turn conformations, respectively.

X-ray Diffraction (XRD) measurements were conducted on a Rigaku Ultima-IV Diffractometer using Ni-filtered CuKα radiation at 40 kV and 30 mA in the range of $2\theta = 4\text{-}40^{o}$ with a scanning rate of $0.6\,^{o}$ /min.

3.4.3 Thremal properties of cryogels and organohydrogels

Differential scanning calorimetry (DSC) measurements were performed on a Perkin Elmer DSC 4000 instrument under a nitrogen atmosphere. Wet cryogel and OHG samples were weighed approximately 10 mg each and placed in aluminum pans, then subjected to two heating-cooling cycles at 0 – 80 °C. As a result of the measurements, the melting enthalpies (ΔH_m) and crystallization degrees (f_{cry}) were determined as previously reported. [101].

3.4.4 Morphological properties of cryogels and organohydrogels

Scanning electron microscopy (SEM) imaging was performed using platinum-coated samples with an FEI-QUANTA FEG 250 FE-SEM peripheral electron microscope. The pore size distribution analysis was performed by taking the diameter measurement data of 50 randomly selected pores from the SEM images with Image-Pro Plus 6 software and creating density distribution curves from the obtained data. [101].

3.4.5 Mechanical properties of cryogels and organohydrogels

Mechanical tests of cryogels and OHGs were carried out on a Zwick Roell test device using a 500 N load cell. Tests were conducted in uniaxial compression mode. Stress (σ_{nom}) – strain (ε) curves were read by applying force at a compression speed of 5 $mm.min^{-1}$ to the wet-swollen materials at room temperature. Young's Modulus values were calculated from the 2 – 4% compression range of the curves. Stress values are expressed as nominal (force applied per unit surface area with respect to the initial surface area of the undeformed specimen), while strain is expressed as the relative change of the specimen with respect to the initial length. When determining the rupture stress (σ_f) and strain (ε_f) values, these quantities were converted to true stress-strain curves as previously reported. [94].

For cyclic mechanical tests, cryogels and OHGs were tested with a waiting period of 5 minutes between loading and unloading cycles. In the tests carried out in two phases, the samples were first compressed and released in 5 consecutive cycles up to a constant 80% maximum strain (ε_{max}). The second phase was carried out in 8 consecutive loading-unloading cycles with 10% increments between 10 - 80% of ε_{max}.

3.4.6 Rheological properties of organohydrogels

Rheological measurements were carried out with the Bohlin Gemini 150 rheometer device with a temperature control feature. A parallel circular measuring plate with a diameter of 20 mm was used and a solvent trap was added to prevent solvent evaporation at high temperatures. OHGs were tested in frequency (ω) sweep test at 25, 65, and 25 ^{o}C, respectively. After the OHG samples, whose rheological tests were performed at 25 ^{o}C, were heated to 65 ^{o}C in a water bath, the test was performed again with the same sample. At the last stage, the sample was left to cool at room temperature and the test was repeated for the third time. The tests were carried out by keeping the constant 0.1% strain (γ_0) value for OHGs and the frequency was varied between 1 and 60 Hz.

3.4.7 Shape memory tests of organohydrogels

OHG shape memory tests were performed using the bending test method. In this method, when cylindrical OHG samples (5 cm in length, 4 mm in diameter) were heated to 65 °C and softened to reshape, they were fixed into a horseshoe-like temporary shape at a certain deformation angle (θ_d) by bending the two ends as if they were meeting.

Then, the samples were kept at 25 ^{o}C for 5 minutes in order to fix this temporary shape. When the force causing deformation is removed, the angle value (θ_f) fixed by the samples was also measured, and the shape fixation ratio (R_f) was determined from the ratio between the two angles.

Finally, the OHGs were reheated to 70 °C without applying an external force on them, the recovery angles (θ_r) were measured at every 1-3 °C range, and the recovery rate (R_r) was calculated.

4. RESULTS and DISCUSSION

In this section, first of all, the preparation of SF cryogels, which constitute the first network structure used as a scaffold in OHG production, their characteristics and the effects of changing SF concentration on the cryogel properties will be presented. Later, the properties of OHGs formed as a result of AAc – C18A copolymer micro-organogel synthesis within the cryogel pores will be explained in detail, and the effects of changing C18A mole fraction on OHG characteristics will be discussed.

4.1 Silk Fibroin Cryogel Scaffodls

4.1.1 Swelling and gel fraction results of cryogels

SF cryogel scaffolds were synthesized at 4 different SF concentrations, namely 5, 10, 15 and 20 w/v % to examine the effect of SF concentration (C_{SF}) on the cryogel properties. 1,4-butanediol diglycidyl ether (BDDE) was used as a crosslinker, and *N*,*N*,*N'*,*N'*-tetramethylethylenediamine (TEMED) was used to adjust the pH of the reaction solution. Table 4.1 and Figure 4.1 show the weight (q_w) and volume (q_v) swelling ratios, gel fractions (W_g) and the total porosity (P) of the cryogels synthesized at various silk fibroin concentration C_{SF}. With an increase in C_{SF} from 5 w/v% to 20 w/v%; total porosity decreases from 92.7 to 74%. Simultaneously, the weight swelling ratio q_w decreases from 11.4 to 4.2% while the swelling ratio by volume remains constant at around unity (Figure 4.1). As mentioned earlier, this behavior is a result of the macroporous structure of the cryogels, in other words, the mass of the cryogel increases significantly due to the filling its pores with water, while the pore walls are not stretched to change the volume [48]. In this study, the term “wet cryogel” was preferred to describe gels in swelling equilibrium in water, since the notation of “swollen cryogel” may suggest gels that are swollen in volume and expanded in size. The gel fraction (W_g) for all cryogels was found to be over 95%.

Table 4.1: Mass (q_w) and volume (q_v) swelling ratios, gel fractions (W_g) and total porosity (P) of cryogels synthesized at various C_{SF}.

C_{SF}, w/v%	q_w	q_v	W_g	P%
5	11.4±1.6	1.062±0.02	1.00±0.23	92.7±1.0
10	6.2±0.8	1.065±0.02	0.96±0.30	86.1±1.6
15	5.27±0.35	1.083±0.02	1.04±0.03	83.4±1.3
20	4.21±0.1	1.385±0.1	1.10±0.04	74.0±2.2

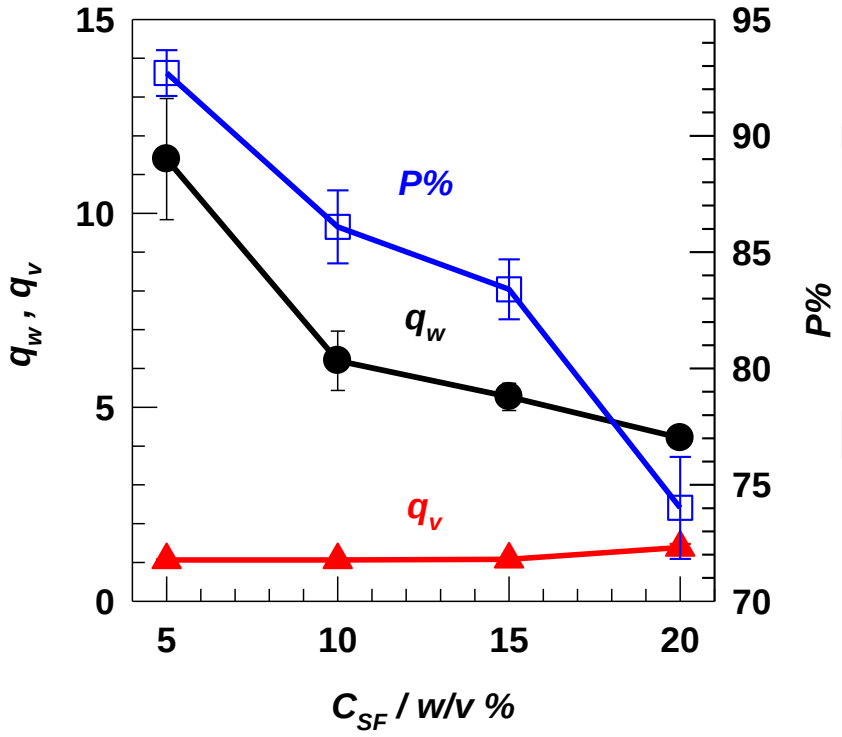

Figure 4.1: Total porosity P of the cryogels, their swelling ratios by volume (q_v) and mass (q_w) plotted against SF concentration C_{SF}.

4.1.2 Morphological and conformational analysis of cryogel scaffolds

Figure 4.2a,b and c shows SEM images of the cryogels formed at various C_{SF} at two different magnifications, also plots average pore sizes at different values and depicts the pore size distribution counts, respectively. Similar to the decrease in total porosity, the decrease in average pore diameters with the increase in C_{SF} is clearly discernible from SEM imaging (Figure 4.2a). On the other hand, it was calculated that the pore

volume (V_p) of spherical pores decreased from 17.4 ± 1.1 to 2.87 ± 0.7 mL g^{-1} as C_{SF} is increased. In Table 4.2 the average pore sizes and the pore volumes of cryogel scaffolds are enlisted.

Table 4.2: Average pore sizes and pore volumes (V_p) of cryogels synthesized at vairous C_{SF} values.

C_{SF}, w/v%	*Pore size, μm*	V_p, *mL.g-1*
5	26±8	17.34±1.11
10	24±7	3.87±0.02
15	21±6	2.91±0.1
20	17±4	2.87±0.68

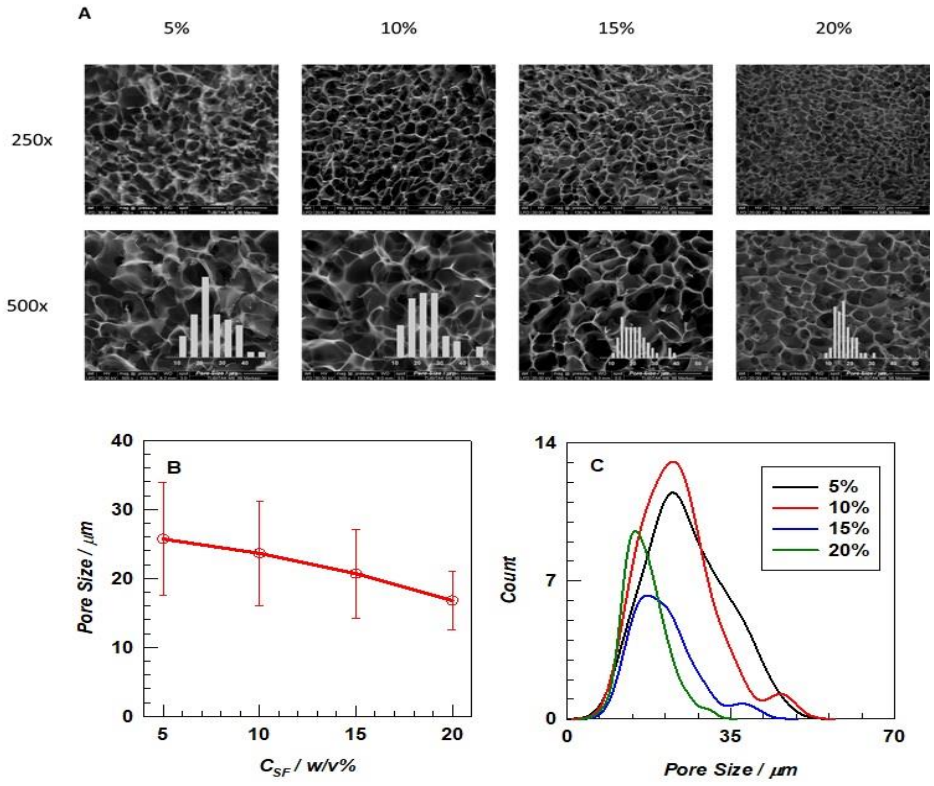

Figure 4.2: Scanning electron microscopy (SEM) images of (a): 250x (top) and 500x (bottom) magnification of SF cryogel scaffolds produced at 5 - 20 w/v% concentrations. (b): Change in the average pore diameters plotted against SF concentration $C_{SF.}$ (c): Pore size distribution curves of various C_{SF} cryogels.

Figure 4.3 shows the FTIR scans of SF before cryogelation, various C_{SF} cryogels, and the distribution ratios of the conformations against C_{SF}. FTIR scans show that with the increase in C_{SF}, the fraction of regulated β-sheet and α-helix conformation increases, while that of disordered random coil conformation gradually decreases. Fig. 4.3a shows the FTIR scan of neat SF solution before it was subjected to the cryogelation reactions. In this curve, the irregular random coil conformation (blue line) visibly occupies the greatest proportion among all others. Compared to this SF absorbance curves, the significant increase in the ratio of β-sheet indicates gelation of fibroin [49]. This is a result of the packing effect of high concentrations of SF chains and forcing them to form more ordered conformations due to the crosslinking with BDDE.

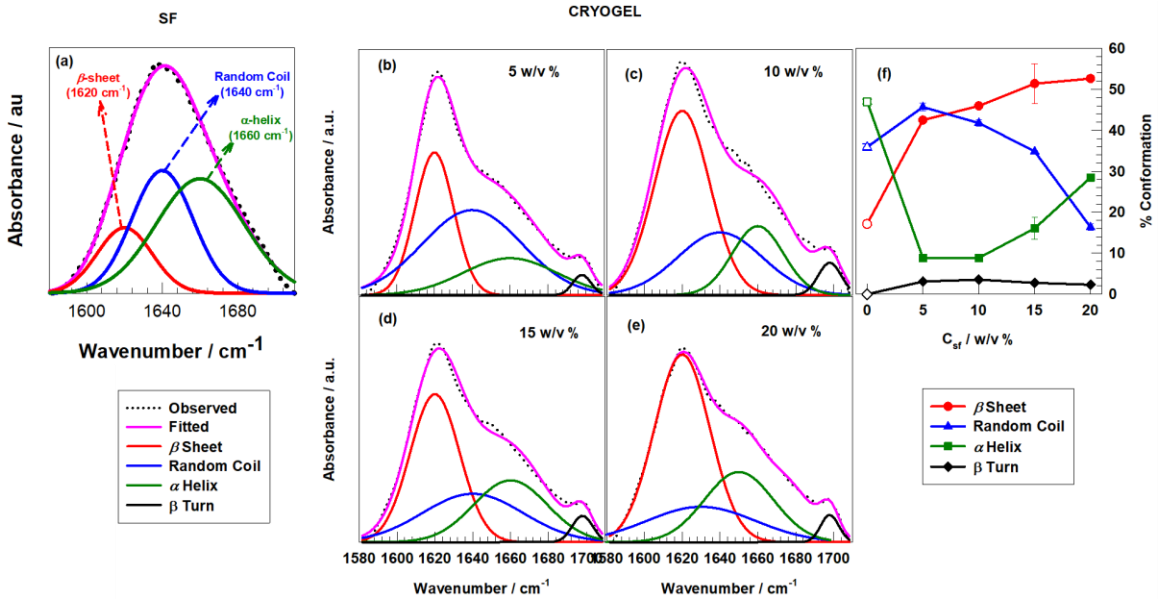

Figure 4.3: (a)FTIR spectrum of SF before cryogelation. (b-e); Amide-I region peaks of FTIR spectra of 5 - 20 w/v% SF cryogel scaffolds. The dotted lines show the raw device measurement, the solid lines show the fitted curve. (f); Variation of β-sheet, random coil, α-helix, and β-turn conformation ratios depending on C_{SF}. Blank symbols represent SF pregelation values.

4.1.3 Mechanical properties of cryogels

Figure 4.4 shows uniaxial compression mechanical test results of wet and dry cryogels. At wet state, cryogels typically do not exhibit any fracture point at their compression stress-strain curves. The actual fracture points of cryogels are determined via converting the nominal (σ_{nom}) stress values into the true (σ_{true}) stress values. The actual fracture points of cryogels are determined at the peak points of the σ_{true} –ε plots [66].

The fracture strain (ε_f) is accepted as the strain value at that point, however, the fractrure (σ_f) stresses are accepted as the corresponding σ_{nom} to this strain values. It was observed that the Young's modulus (E) and toughness (W) values of the cryogels after freeze drying increased by 100 times compared to the wet condition, and the toughness (W) values increased by 10 times (Figure 4.4h). The increase in Young's modulus and toughness values with increasing C_{SF} shows that the mechanical stability of SF cryogels increases as a result of decreased porosity and thickening of the pore walls [41]. The reason for the plateau regions in the stress-strain curves for both wet and dry cryogels as seen in Figure 4.4a,c,d is the collapse of their pores due to the compression. The collapsed pores cause volume reduction and, in this process, the cryogels are compressed, but the water-air coming out does not create a tension response, so the graph in this region looks like a horizontal plateau.

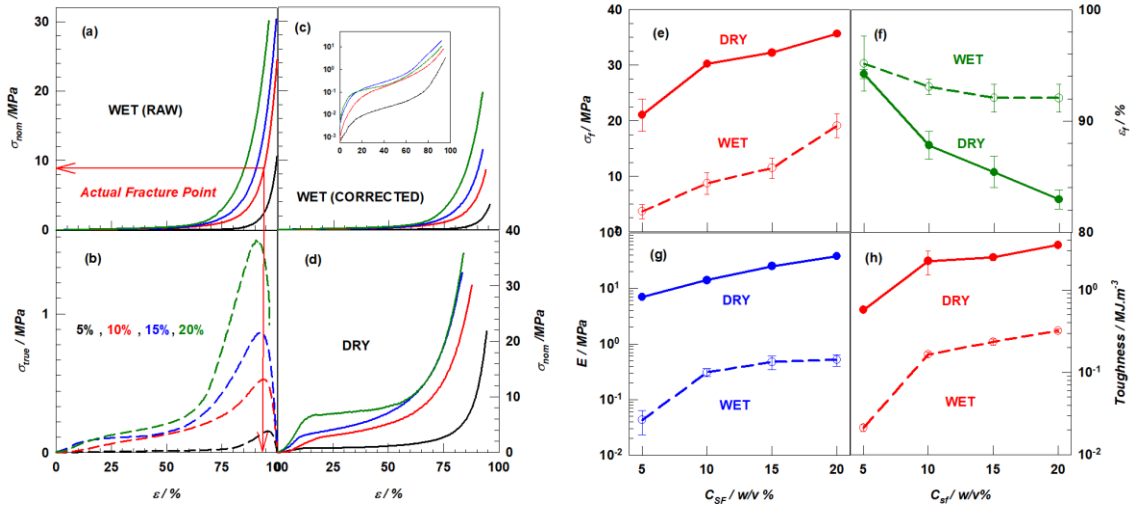

Figure 4.4: (a) Wet SF cryogels' nominal stress σ_{nom}-strain ε plots. (b) Wet SF cryogels' nominal stress true stress σ_{true} – strain ε plots. (c) Wet SF cryogels' corrected nominal stress σ_{nom} – strain ε plots. (d) Dry SF networks' nominal stress σ_{nom} – strain ε plots. The red arrows are representations of fracture stress σ_f and strain ε_f in the wet state determined at the peaks of the σ_{true} - ε curves. Comparative change in the fracture stress σ_f (e), fracture strain ε_f (f), Young's modulus E (g), toughness W (h), values at dry (solid line, solid symbols) and wet states (dashed line, empty symbols) as a function of C_{SF}.

The ability of SF cryogels to be compressed up to 95% of their initial length without breaking and to exhibit much higher shear stresses than hydrogels[41] stems from the 'cryoconcentration' effect, which gives cryogels durable and elastic pore walls as well

as interconnected macropores [40-41,102]. This phenomenon refers to the accumulation of solutes in apparently frozen solutions and being trapped in small volumes in unfrozen regions. According to this principle, the components of the cryogel precursor solution are trapped in micron-sized unfrozen channels, increasing their concentrations up to the suitable for cryogelation reactions and cross-linking and gel formation occur due to this effect. Previous studies have shown that the cryoconcentration effect increases the concentration of the gel components in unfrozen channels by approximately 5.8 times. [41]. This effect engenders the gelation reactions, leads to conformational arrangements in the SF chains, and creates stronger and more elastic pore walls than hydrogels. With their superior mechanical properties, cryogels are very valuable first networks in OHG production.

4.2 Organohydrogels

4.2.1 Synthesis of organohydrogels

In organohydrogel (OHG) synthesis, there are four approaches specified in the literature as mentioned above. For example, Gao et al. applied a bi-step OHG production approach, the hydrophilic first phase was fabricated from poly(*N*,*N*-dimethyl acrylamide) hydrogel, then OHG was produced by filling the organogel into these hydrogel pores, which were dehydrated with a freeze dryer [96]. In a recent publication, a similar application utilizing heteronetwork strategy was used by our research group for methacrylate SF-DMAA cryogel first network OHGs [98]. In the present study, with a similar approach, a hydrophilic SF cryogel was first freeze-dried to produce a macroporous scaffold and then its pores were filled with an organogel precursor solution (ethanolic phase containing AAc/C18A monomers, BAAm crosslinker and AIBN initiator) and held for 24 h at 50 ^{o}C to produce OHGs via free radical polymerization. SF cryogels were preferred as a hydrophilic skeleton structure, due to the interconnected macroporous structure and mechanical superiority of cryogels, as explained previously.

Within the scope of the study, SF concentration (C_{SF}) of the starting cryogels were varied in order to examine the effect of C_{SF} on the mechanical and viscoelastic properties of OHGs. The mole fraction of C18A monomer (x_{C18A}) was also varied

between 0.1 and 0.3. In our experiments, the total monomer concentration (C_0) in the organogel precursor solution was fixed at 41 w/v%. BAAm and AIBN were used as 1 mol% with respect to the total monomer amount.

4.2.2 Organogel precursor intake capacity of SF cryogel scaffolds

In the synthesis stage, in order to investigate the influence of monomer solution uptake capacity of the SF cryogel porosity, firstly, swelling properties of dry cryogels in monomer solution were investigated. Similarly to the water swelling, while the cryogels swelled in the ethanol phase, the volume did not change, but they swelled by weight. Consequently, the swelling ratio by mass in the monomer solution $q_{w,o}$ was defined. This value was calculated in the same way as the swelling ratio by mass in water. Fig. 4.5a shows $q_{w,o}$ of the cryogels immersed in monomer solutions of various C18A contents (x_{C18A}) plotted against the fibroin concentration C_{SF}. It is seen that the solution uptake capacity rapidly decreases with increasing C_{SF} from 5 to 10 w/v%. Further increase in C_{SF} does not change much the uptake capacity qwo and remains around 3. Moreover, C18A content (x_{C18A}) of the solution also affect the uptake capacity at C_{SF} = 5 w/v%. The higher x_{C18A}, the higher $q_{w,o}$ revealing that increasing C18A content of the solution also increases the uptake capacity of the cryogels formed at C_{SF} = 5 w/v%.

For synthesis, dry cryogel scaffolds were kept in monomer solution for 10 minutes under mechanical stirring and their pores were completely filled with the solution. Then, the filled cryogels and excesive precursor solution were taken into plastic syringes and kept at 50 °C for 24 hours to perform thermal radical polymerization. Thus, OHGs based on SF cryogel scaffolds containing poly(AAc-co-C18A) micro-organogels in their pores were obtained. After the synthesis, OHGs were thrown into ethanol and the unreacted components were removed from the structure. After that, they were kept in water until the swelling equilibrium was reached. The gel fraction (W_g) for all OHGs was found to be around 1.

For post-synthesis stage OHGs, the mass fractions of the organogel part ($w_{organogel}$) and C18A units (w_{C18A}) regarding to OHG were calculated according to equations 4.1 and 4.2, respectively.

$$w_{organogel} = \frac{(q_{w,o} - 1)C_0}{1 + (q_{w,o} - 1)C_0} \quad (4.1)$$

$$w_{C18A} = w_{organogel} m_{C18A} \quad (4.2)$$

Here, m_{C18A} is the mass fraction of C18A in the monomer mixture.

Figure 4.5b and 4.5c show the variation in $w_{organogel}$ and w_{C18A} against C_{SF} for various OHGs. It is seen that for OHGs with constant 5 w/v% C_{SF}, $w_{organogel}$ increased from 61% to 80% with increasing x_{C18A}. For OHGs with constant 0.3 x_{C18A}, $w_{organogel}$ is decreased from 80% to 36% with increasing C_{SF} from 5 to 20 w/v%. It can be said that the increased C_{SF} and the corresponding decrease in pore diameters caused a decrease in the organogel integration ability. However, w_{C18A} increases with increasing x_{C18A} for each C_{SF} value cryogel (Fig. 4.5c). This is an expected outcome, since the mole fraction, thus mass percentage of C18A increases corresponding to the x_{C18A}, and drop in the average pore size of cryogels results in a proportionate drop in the organogel intake capability of the scaffold. In Figure 4.5d-g, swelling values by mass (q_w) and volume (q_v) of OHGs in water and ethanol are shown in comparison with empty cryogels (dashed lines). The q_w values of cryogels in both water (Fig. 4.5d) and ethanol (Fig. 4.5f) showed a significant decrease especially for cryogels with C_{SF} = 5 w/v% after conversion to OHG. At this time, w_{C18A} decreased significantly with increasing x_{C18A} for all OHGs.

Figure 4.5e and 4.5g show the swelling by volume (q_v) raitos of OHG within water and ethanol, respectively. Cryogel and OHG q_v values converge with increasing C_{SF} values. Similarly, it is seen that increasing x_{C18A} values decrease the swelling ratio. Conversely, the swelling ratios by volume were found to be higher for OHGs than for cryogels. It can be thought that this increase is due to the hydrophilic AAc units formed in the OHG structure. However, ethanol is a better solvent than water for OHGs, the majority of which is poly(AAc-co-C18A) organogel [103]. As a result, it was observed that OHGs swell relatively better by both mass and volume in ethanol. Figures 4.5h and 4.5i show the variation of total percent porosity (*% P*) and pore volume (V_p) with respect to C_{SF}. For OHGs with increasing C_{SF} values, *P%* values decreased from 45.1 to 8.1 % and the V_p values varied between 0.26 – 0.16 mL.g^{-1}. For OHGs with

increasing x_{C18A} vlaues, $P\%$ increased from 92.7 to 45.1 % and V_p decreased from 17.33 to 0.16 mL.g^{-1}. While V_p values do not change much with C_{SF}, they differ significantly with increasing x_{C18A} values. Corresponding values were enlisted in the Table 4.3.

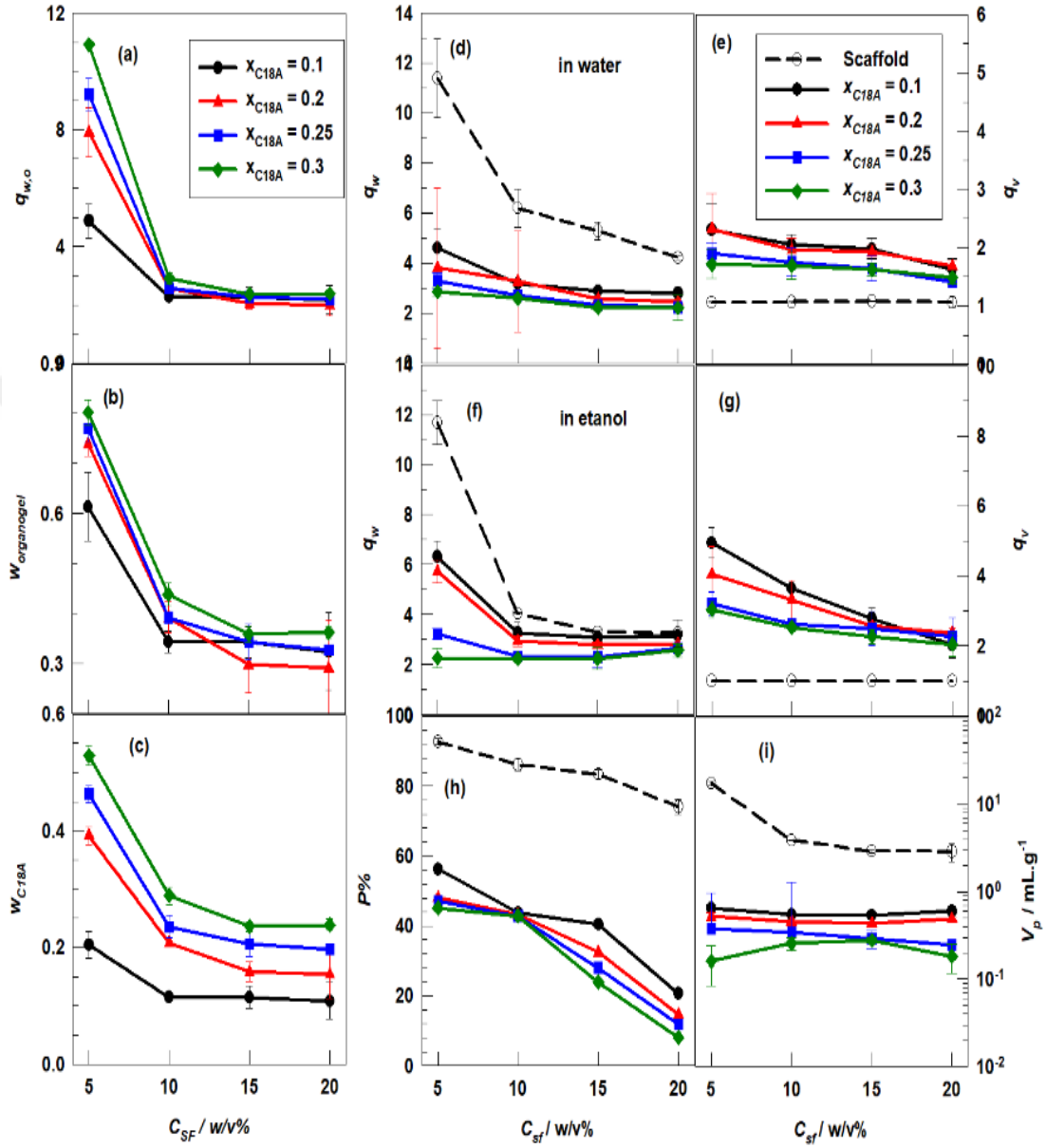

Figure 4.5: Mass swelling ($q_{w,o}$) ratio of cryogels in the organogel precursor solution, (a); mass fraction of the organogel part in OHG ($w_{organogel}$), (b); Mass fraction of C18A units in OHG (w_{C18A}). Cryogel and OHGs in water swelling ratios, by mass q_w (d) and by volume q_v (e). In ethanol swelling ratios by mass q_w (f), and by volume q_v (g). Total percent porosity $\%P$ (h), total pore volume V_p (i). The dashed lines represent the neat SF cryogel values.

Table 4.3: The swelling ratio by mass in the monomer solution ($q_{w,o}$), the mass fractions of the organogel part within OHGs ($w_{organogel}$), the mass fractions of the C18A within the OHGs (w_{C18A}), total percent porosity of OHGs ($P\%$) and pore volume of the OHGs (V_p) for several OHGs produced.

Gel Code	$q_{w,o}$	$w_{organogel}$	w_{C18A}	$P\%$	V_p, $mL.g^{-1}$
501	4.87±0.59	0.61±0.07	0.2±0.02	56±1	0.65±0.08
502	7.92±0.85	0.74±0.02	0.39±0.01	48±1	0.52±0.08
525	9.22±0.55	0.77±0.03	0.46±0.01	47±1	0.37±0.6
530	10.93±0.07	0.80±0.02	0.53±0.02	45±1	0.16±0.07
1030	2.91±0.17	0.44±0.02	0.29±0.01	43±1	0.25±0.04
1530	2.36±0.07	0.35±0.01	0.24±0.01	24±1	0.27±0.02
2030	2.38±0.09	0.36±0.01	0.24±0.01	8±1	0.18±0.07

4.2.3 Morphological analysis of organohydrogels

Figure 4.6 shows SEM images of the cryogel scaffolld prepared at 5 w/v% SF concentration (left), and the OHG derived from it at a C18A fraction x_{C18A} of 0.30. The images show that the pore cavities of the initial cryogel scaffold are clearly visible as black shadowy pits separated by white pore walls while after converting it to OHG, these regions are seen as gray-opaque meaning that the pores filled up and appeared to be closed.

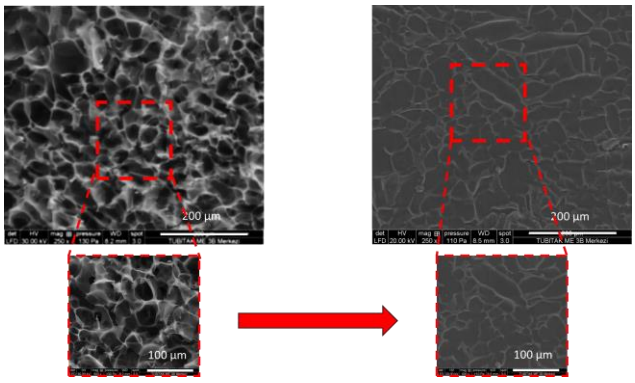

Figure 4.6: SEM images of cryogel used in OHG synthesis at C_{SF} = 5 w/v% value (left) and OHG with 5 w/v% C_{SF} and 0.3 x_{C18A}. produced from this cryogel (right). The scale bar is 200 μm.

Figure 4.7 shows SEM images of OHGs formed at various SF and C18A concentrations. The upper panel in the figure shows the images of OHGs formed at C_{SF}= 5 w/v% and at various x_{C18A} between 0.10 to 0.30 (from right to left). In the bottom panel, the images are for OHGs prepared at a fixed x_{C18A}. In all OHGs, it is clearly seen that almost all the pores are closed and the pore walls are covered with micro-organogel structure. It can be seen that organogels with increasing x_{C18A} values filled the pore cavities more and OHGs with x_{C18A} = 0.3 were completely filled and closed (Figure 4.7-top). For increasing C_{SF}, it was observed that the pore walls became more obscure and their depth disappeared completely (Fig. 4.7-bottom).

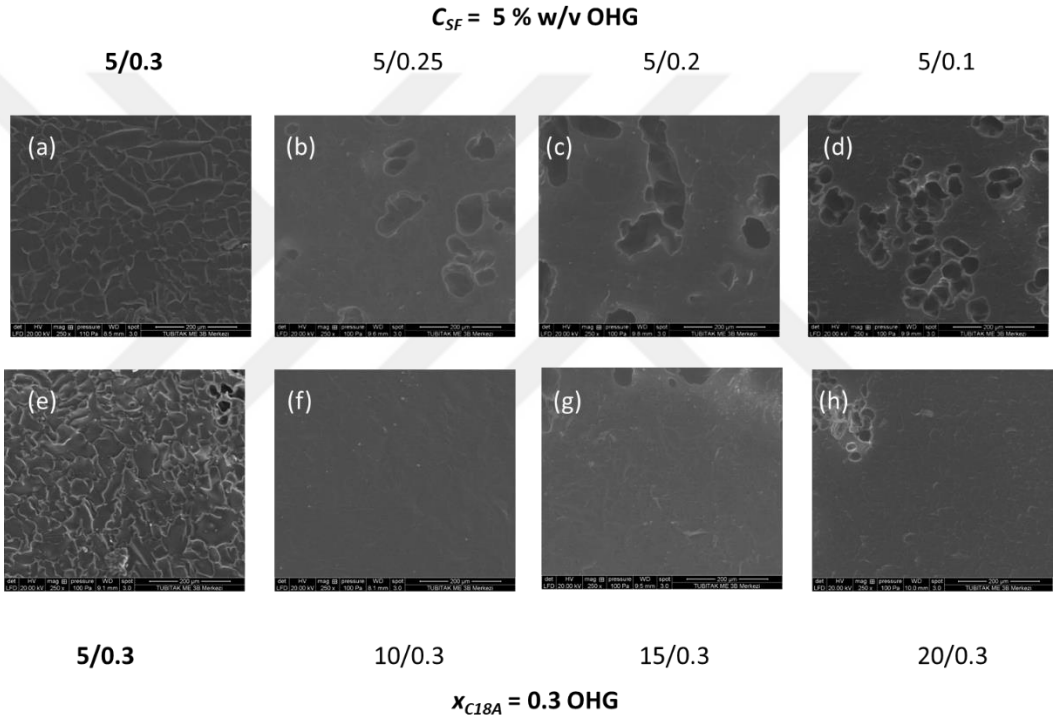

Figure 4.7: SEM images of OHGs with constant 5 w/v% C_{SF} and increasing x_{C18A}. (a-d) and with constant 0.3 x_{C18A} and increasing C_{SF} (d-g). Scale bar is 200 μm.

4.2.4 Thermal, vicoelastic and mechanical properties of organohydrogels

It has been demonstrated in previous studies that semicrystalline gels containing hydrophobic comonomers have temperature-dependent tunable viscoelastic and mechanical properties [104–106]. In this part of the study, poly(AAc-co-C18A) semicrystalline organogels formed in μm-sized SF cryogel pores were investigated to whether they possess a structure that can be melted and crystallized reversibly with the effect of temperature, and have given tunable properties to them by differential

scanning calorimetry (DSC) tests. Then, their rheological behavior was examined under different temperatures and the effect of temperature on mechanical properties was revealed. Finally, the effect of crystalline regions formed at room temperature on OHG mechanical properties was demonstrated by performing uniaxial mechanical compression tests.

Figure 4.8 shows the DSC thermograms of OHGs prepared at different x_{C18A} (a,c) and C_{SF} (b,d) values. For comparison, the thermogram of the starting cryogels are also given in the figure by the black curves. As expected, no melting or crystallization peaks are seen in the thermogram of the cryogels, but as a result of micro-organogel filling, a peak of varying intensity and sharpness appears in OHGs depending on the amount of C18A were obtained. Thermogram results showed progressively growing and sharpening melting peaks with increasing x_{C18A} from 0.1 to 0.3 (Figure 4.8a).

It was observed that the crystallization peaks became sharper and larger with increasing x_{C18A}. There was no crystallization peak in the cooling thermogram of OHGs with 5 w/v% C_{SF} and 0.1 x_{C18A} only (Figure 4.8c). This observation was attributed to the steric hindrance of the cryogel scaffold during crystallization in these OHGs with the lowest melting crystallinity ratio (f_{cry}). It was observed that the melting temperature (T_m), which is the temperature measured at the peak of the melting curves, varies from 41.8 ± 1 to 53.7 ± 1 ^oC, and the crystallinity temperature (T_c), which is the temperature measured at the peak of the descending crystallization curves, increased from 42.1 ± 1 to 45.9 ± 1 ^oC (Fig. 4.8g).

For OHGs with increasing C_{SF} and constant 0.3 x_{C18A}, it was observed that the melting and crystallization peaks shrunk with increasing C_{SF} amounts, while the peaks appeared at around 52 and 44 ^oC for melting and crystallization, respectively (Figure 4.8b,d,h). Black dashed lines at the bottom represent the DSC thermograms of the poly(AAc-co-C18A) organogel measured and plotted as a reference.

Figures 4.8e and 4.8f show the crystallization degrees (f_{cry}) of OHGs plotted against x_{C18A} and C_{SF}, respectively. It was calculated that for OHGs with increasing x_{C18A} and constant 5 w/v% C_{SF}, f_{cry} increased between 2 and 15.7% with increasing x_{C18A}. On the

other hand, while this value was 16.3% in organogels without SF cryogel, it decreased between 15.7 and 2.9% with increasing C_{SF} value after conversion to OHG.

These results show that x_{C18A} affects f_{cry}, T_m and T_c of OHGs, while the change in C_{SF} affects only f_{cry}. The degree of crystallization (f_{cry}) is, by definition, an expression of the amount of C18A capable of forming a crystalline region as a function of x_{C18A}.

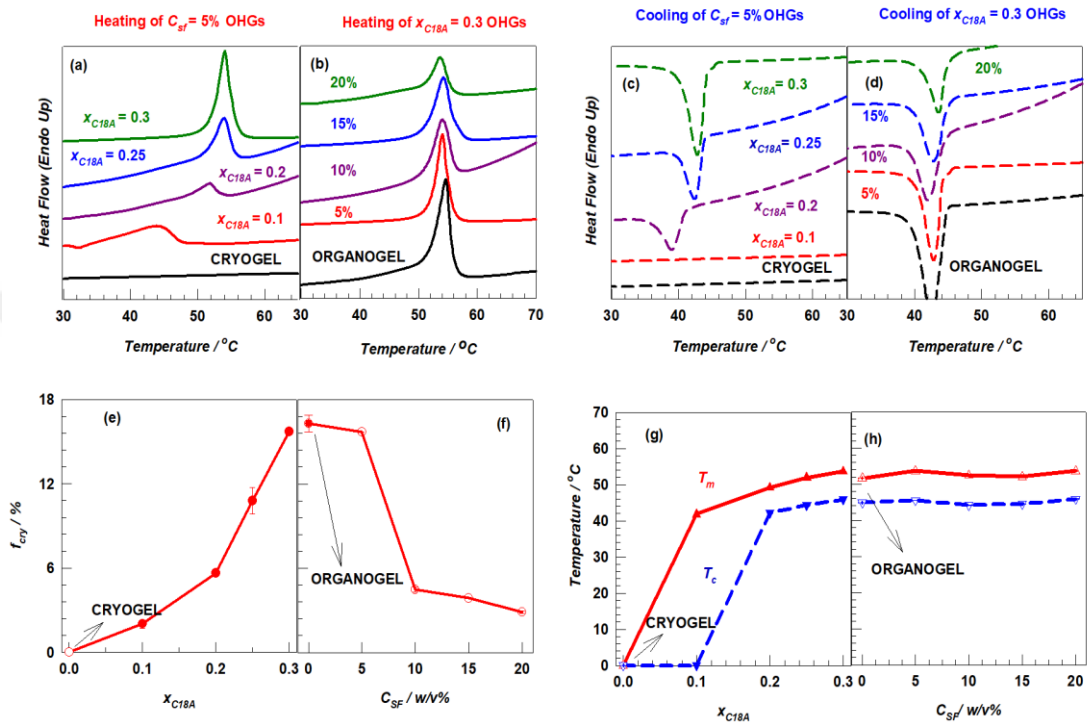

Figure 4.8: (a) Heating DSC thermograms of OHGs with constant 5 w/v% C_{SF} and increasing x_{C18A}. Black line represents the wet cryogel thermogram for comparison. (b) Heating DSC thermograms of OHGs with constant 0.3 x_{C18A} and increasing C_{SF}. Black line represents the x_{C18A} = 0.3 organogel thermogram for comparison. (c) Cooling DSC thermograms of OHGs with constant 5 w/v% C_{SF} and increasing x_{C18A}. Black line represents the wet cryogel thermogram for comparison. (d) Cooling DSC thermograms of OHGs with constant 0.3 x_{C18A} and increasing C_{SF}. Black line represents the x_{C18A} = 0.3 organogel thermogram for comparison. Crystallinity ratios (f_{cry}) of OHGs plotted against x_{C18A} (e) and C_{SF} (f). Melting temperature (T_m) and crystallization temperature (T_c) plotted against x_{C18A} (g) and C_{SF} (h). The solid line represents T_m and the dashed line represents T_c.

In this context, as expected, the amount of C18A units that can form crystalline regions in the OHG structure increased with C18A mole fraction, so naturally, the f_{cry} values do. Because this value is a quantitive indication of the crystalline regions formed within the structure. The change in T_m and T_c, however, is influenced by the the

quantity of repeating hydrophobic units in the crystalline regions. The number of repeating C18A units forming crystalline regions increases with x_{C18A}. This increase leads to intensification of hydrophobic interactions in the crystalline regions. Higher T_m 's are observed, as a higher energy is required to disperse these strengthened crystalline structures. Likewise, as the OHGs' temperature decreases from above T_m to a value below T_c, the hydrophobic interactions of OHGs with constant 0.3 x_{C18A} and increasing C_{SF} that have crystalline regions composed of many repeating C18A units very rapidly rearrange the crystalline regions, so these OHGs crystallized at the highest T_c values. are. The f_{cry} values of OHGs were measured to be lower than previously reported AAc-C18A hydrogels [104-105]. This difference suggests that the C18A hydrophobic tail side chains within the pores are less oriented to form the crystalline region. This is most probably an outcome of the steric hindrance of the intrusive cryogel pore walls that were amidst the micro-organogel second network.

Figure 4.9 shows the X-ray diffraction (XRD) patterns of cryogel scaffolds of different C_{SF} and OHG with 5 w/v% C_{SF} and 0.1 x_{C18A}, OHGs with constant 0.3 x_{C18A} and increasing C_{SF} and also the x_{C18A} = 0.3 organogel comparatively.

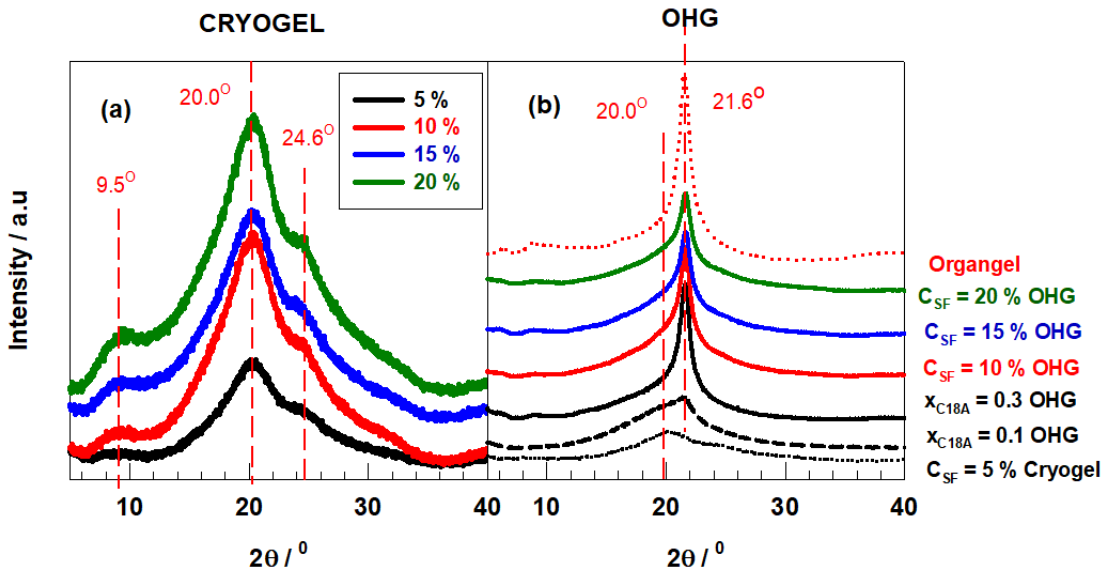

Figure 4.9: (a) XRD patterns of cryogels synthesized at C_{SF} = 5 – 20 w/v%. (b) XRD patterns of 5 w/v% C_{SF} cryogel, OHG with 5 w/v% C_{SF} and 0.1 x_{C18A} (dashed

line), OHGs with constant 0.3 x_{C18A} and increasing C_{SF} and also the x_{C18A} = 0.3 organogel produced at x_{C18A} = 0.3 included for comparison at 2θ = 4-40° region.

The peaks at 9.5°, 20° and 24.6° are seen in the XRD patterns, which are typical for the β-folded structure of fibroin. The sharpening of the peaks with increasing CSF indicates an increase in the β-sheet ratio with increasing fibroin concentration, which is in accord with previous results [107–109]. XRD patterns of OHGs prepared at various C_{SF} and x_{C18A} are shown in Figure 4.9b. A peak at around 21.6° corresponding to a *d*-spacing of 0.41 nm appears for all OHGs, and it sharpens gradually with increasing C_{SF} or x_{C18A}. This peak corresponds to the distance between the C18A side chains oriented perpendicular to the linear organogel chains in the OHG structure [101,105]. It was seen that the flatness of the peaks increases with increasing C_{SF} value. This is probably due to the difficulty of arranging the crystalline regions due to the narrowing of cryogel pores. These findings are accordant with the FTIR and DSC results.

Figure 4.10 shows the angular frequency sweep (ω) test of OHG with 5 w/v% C_{SF} and 0.3 x_{C18A} at 25 °C (Fig. 4.10a), 65 °C (Fig. 4.10b) and again at 25 °C (Fig. 4.10c), respectively. This test was conducted in order to demonstrate the temperature-induced reversible softening and hardening of OHGs. The crystalline regions of OHG that can melt and regenerate reversibly with temperature give it mechanical and viscoelastic properties that differ above and below the melting temperature.

Elastic modulus G' for OHG at 25 °C at swelling equilibrium decreased approximately 6.8 fold (1.49 MPa to 0.219 kPa) after initial heating from 25 °C to 65 °C, when OHG was cooled back to 25 °C has recovered to its initial level. At 65 °C heated stage, it is observed that G' increases from 182 kPa to 248 kPa with increasing ω. The tan δ value, which expresses the ratio of the viscous modulus (G'') to the elastic modulus, increases from 0.36 to 0.4 with increasing frequency at heated stage.

Also it was seen decreased from 0.4 to 0.12 upon heating, form 25 to 65 °C. These values reveal that both elastic and viscous moduli are sensitive to angular frequency above the melting temperature. In addition, the recovery of the initial G', G'' and tan δ

values at 25 °C after cooling stage reveals that the OHGs have reversibly adjustable properties depending on the temperature.

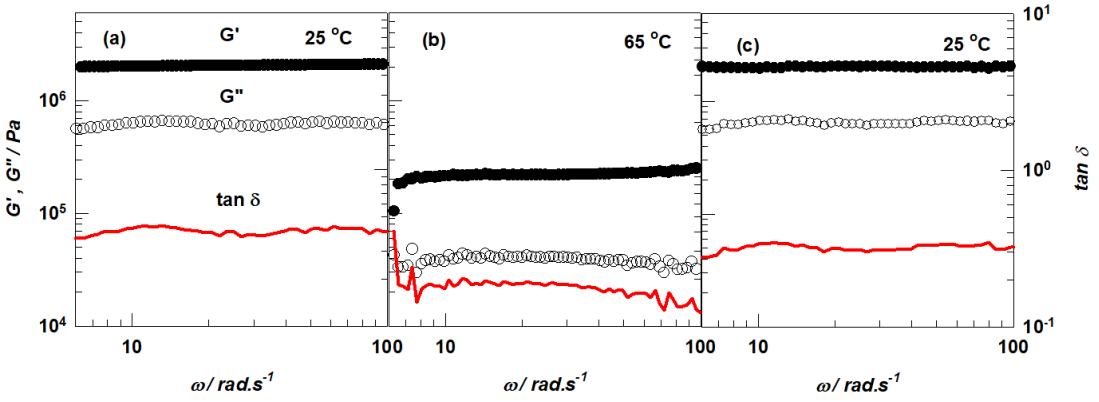

Figure 4.10: Rheological angular frequency (ω) sweep measurements of OHG with 5 w/v% C_{SF} and 0.3 x_{C18A} at 25 °C (a), 65 °C (b) and again at 25 °C (c). Solid and hollow symbols represent G', G'' and the red line represents tan δ values, respectively. γ_0 = 0.1%.

Mechanical properties of OHGs were measured at room temperature by uniaxial compression tests. Figure 4.11a shows representative stress-strain curves of OHG with 5 w/v% C_{SF} and 0.3 x_{C18A} and its organogel and hydrogel constituents. As seen in the inner figure, the toughness (W) of the OHG is 5.32 ± 0.1 MJ.m^{-3}, which is approximately 3 and 24 times higher than the toughness of its individual organogel and cryogel constituents (1.77 ± 0.16 and 0.22 ± 0.02 MJ.m^{-3}, respectively).

In order to investigate the effect of C_{SF} and x_{C18A} parameters on mechanical properties, OHGs with constant 0.3 x_{C18A} and increasing C_{SF} were used for C_{SF} relevancy tests, and OHGs with constant 5 w/v% C_{SF} and increasing x_{C18A} were used to determine the relation of x_{C18A} values with mechanical behaviour. Figures 4.11b and 4.11c show representative stress-strain curves of OHGs at increasing x_{C18A} and C_{SF} values, respectively. The built-in figures are close-up views of the initial low-stress regions. It was seen that conversion of cryogels to OHG significantly improved their mechanical properties. For example, Young's Modulus (E) increased 137-fold (0.043 ± 0.02 MPa to 5.9 ± 0.5 MPa) after conversion of C_{SF} = 5 w/v% cryogel to OHG with 5 w/v% C_{SF} and 0.3 x_{C18A}, the fracture stress (σ_f) increased 8-fold (from 3.64 ± 1.3 MPa to 29.8 ± 0.8 MPa).

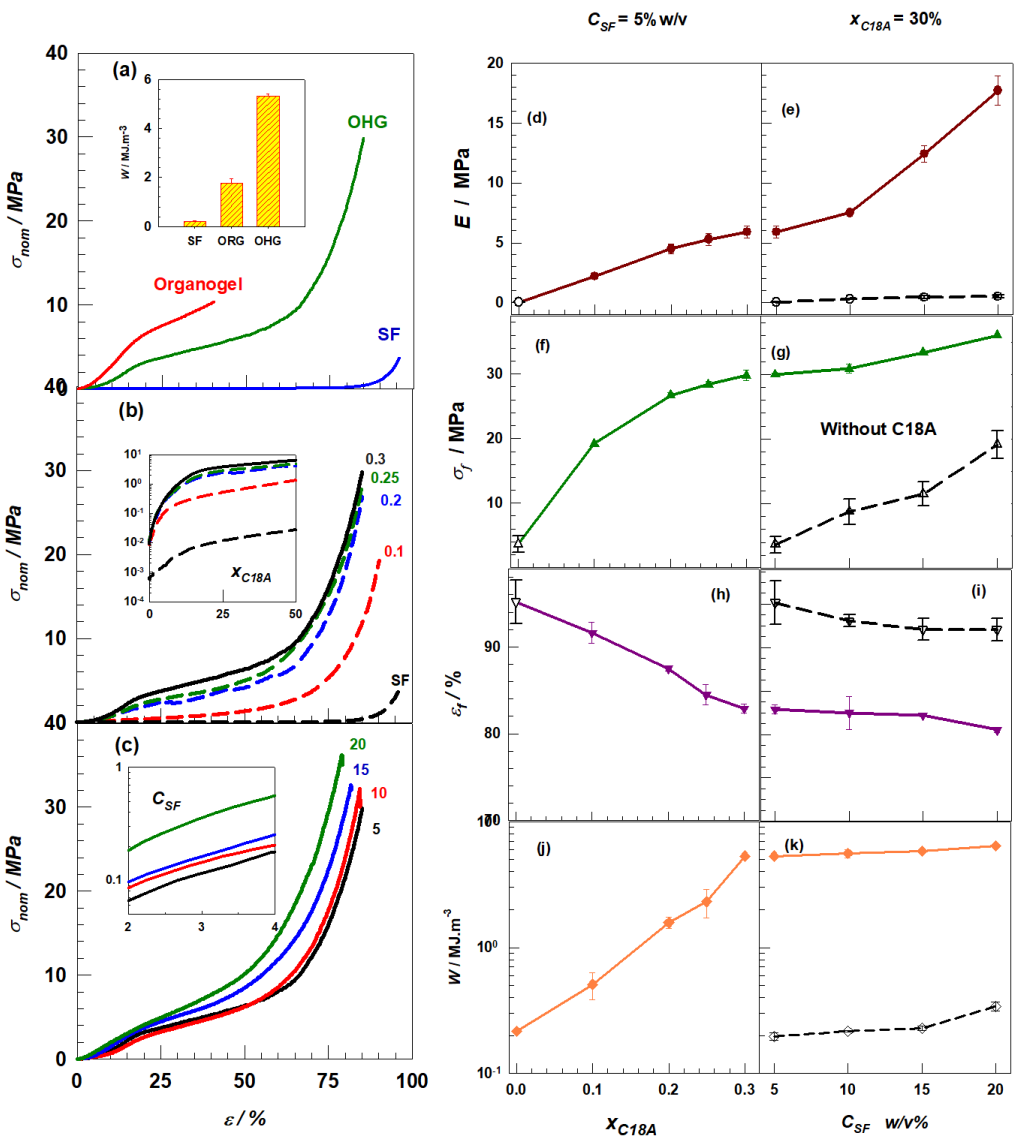

Figure 4.11: (a) Representative stress - strain curves for wet SF cryogel, organogel and OHG. (b) Stress-strain curves of OHGs 5 w/v% C_{SF} and increasing x_{C18A}. The dashed black line represents the reference wet cryogel. (c) Stress-strain curves of OHGs with constant 0.3 x_{C18A} and increasing C_{SF}. Young's modulus E, fracture stress σ_f, fracture strain ε_f, toughness W values plotted against x_{C18A} (d,f,h,j). and C_{SF} (e,g,i,k), respectively. The dashed lines represent the wet cryogel values as a reference.

It was observed that the values of E, W, σ_f are all increased with increasing x_{C18A}, while the fracture stress (ε_f) values exhibited a little drop but still remained above 80%. These improvements are due to the formation of crystalline regions in the micro-organogels formed within the cryogel pores. In addition, increasing x_{C18A} also increased the

plateau stress of OHGs (Figure 4.11b, in-figure). This finding shows that the x_{C18A} ratio has a supportive effect on pore strength and durability. The obtained results revealed that the OHGs produced within the scope of our study have superior mechanical properties than cryogels [110–112] and OHGs [97,113–117] previously reported in the literature.

The considerable increase in mechanical properties, particularly *W*, in OHGs suggests that the cryogel skeleton has developed a much more efficient energy dissipation ability as a result of conversion to OHG. While micro-organogels, which are the discontinuous structure forming OHG, act as a second network, just as in double-network gels containing sacrificable fragile components under mechanical deformation affecting on OHG [92,93] the cryogel scaffold, which is the continuous phase, undertakes the task of maintaining integrity To further elucidate this mechanism, OHGs were subjected to cyclic mechanical tests with sequential loading and unloading steps up to 80% maximum compression strain (ε_{max}).

In Figure 4.12 cyclic mechanical test plots of regular wet cryogels synthesized at different C_{SF} ratios and OHG with 5 w/v% C_{SF} and 0.1 x_{C18A} are given. Figure 4.12a,b shows the representative curves of tests of C_{SF} = 5 w/v% cryogels for 5 of loading-unloading cycles and for 8 cycles with progressive increments of 10%, reaching 80% ε_{max} and for 5 loading-unloading cycles up to the constant 80% ε_{max}, respectively. In zoom in-figures, the hysteresis energies (U_{hys}), calculated as the area between the loading and unloading curves of the cryogels at different C_{SF} values in the relevant tests, are shown as a function of ε_{max} and the number of cycles.

Figure 4.12 c,d shows the representative curves of tests of OHGs with 5 w/v% C_{SF} and 0.1 x_{C18A}, for 5 of loading-unloading cycles and for 8 cycles with progressive increments of 10%, reaching 80% ε_{max} and for 5 loading-unloading cycles up to the constant 80% ε_{max}, respectively. Here, in the in-figures, the U_{hys} values of 5 w/v% (circle) and OHG with 5 w/v% C_{SF} and 0.1 x_{C18A} made with this cryogel are given in comparison. In all figures, solid lines show loading and dashed lines show unloading curves.

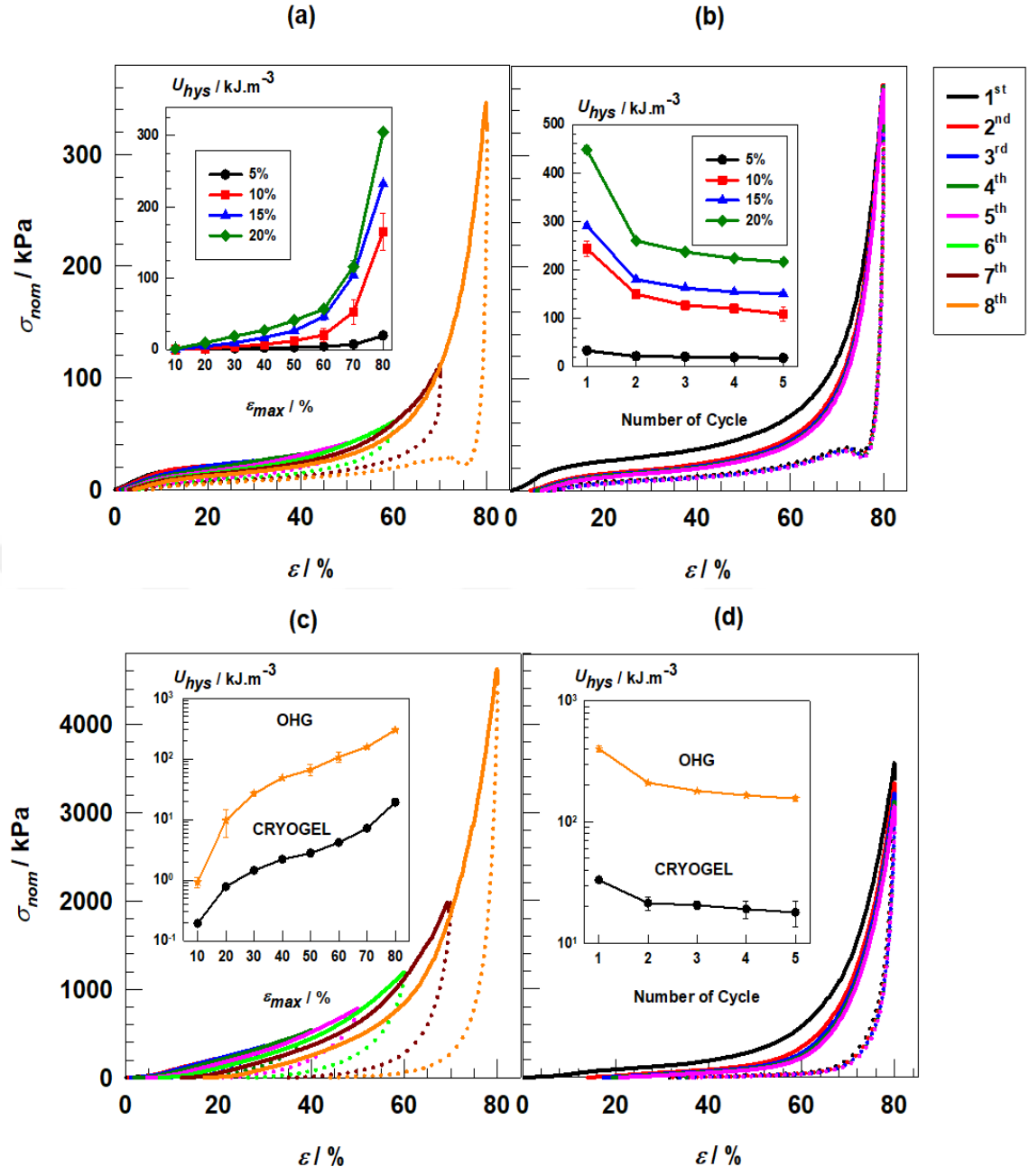

Figure 4.12: Representative cyclic mechanical test plots of (a) C_{SF} = 5 w/v% cryogel and (c) OHGs with 5 w/v% C_{SF} and 0.1 x_{C18A}, reaching 80% maximum compression ratio (ε_{max}) with 8 loading-unloading cycles with successive 10% increments. Zoom in-figures show (a) change in the hysteresis energies (U_{hys}) of different cryogels as a function of ε_{max} and (c) change in the U_{hys} of cryogel and OHG as a function of ε_{max}. Representative cyclic mechanical test plots of (b) C_{SF} = 5 w/v% cryogel and (d) OHG with 5 w/v% C_{SF} and 0.1 x_{C18A}, with 5 consecutive cycles at a constant 80% maximum compression ratio (ε_{max}). In-figures express (b) change in the hysteresis energies (U_{hys}) of different cryogels as a function of ε_{max} and (d) change in the U_{hys} of cryogel and OHG as a function of ε_{max}.

The cyclic test results reveal that $U_{hys,}$ for cryogels, increases with increasing C_{SF} value. The U_{hys} value is a measure of the energy dissipation ability of gels. The increased energy dissipation ability of cryogels is mainly due to the friction between the pore walls of compressible cryogels and the water entering and leaving the pores [66]. The pore walls of macroporous cryogels are not stretched and brittle in the wet state, unlike swollen hydrogels. They also have very thick and steady pore walls compared to hydrogels. These walls preserve their structural integrity as the pores collapse under mechanical deformation and reopen when the tension is removed, just like a sponge. In the meantime, a friction occurs between the water that comes out of the pores and fills back, and this provides the cryogels with an effective energy dissipation mechanism. With increasing C_{SF}, the average pore sizes decreased and the pore walls thickened, thus the surface area of the pore walls that created friction with water increased. This creates a gradually improving energy dissipation mechanism. In fact, the highest amount of SF, C_{SF} = 20 w/v% cryogels, U_{hys} values are even above OHGs'. However, the U_{hys} values of OHG were found to be much higher than the cryogel from which it was produced. This effect is due to the fact that the fragile organogel structure sacrifices itself and disintegrates at the microscopic level and help OHG to maintain its structural integrity, dissipating the deformation energy while OHG when it is exposed to a deformative stress.

4.2.5 Shape memory tests of organohydrogels

Due to their semi-crystalline structure resulting from poly(AAc-co-C18A) micro-organogels, all OHGs produced have shape memory properties at values above the melting temperature (T_m) of the crystalline regions. In order to demonstrate this, OHGs produced in cylinders with a diameter of 5 mm were subjected to shape memory testing by fixing temporary horseshoe-like shapes by end-to-end bending method. Figure 4.13 shows the shape recovery test with permanent, fixed and recovered shapes and shape memory test results. Figure 4.13a-c shows images of an OHG specimen during the bending shape memory test. In (a), OHG is initially in the form of a straight rod (θ_0 = 180^o). After being heated to 65 °C, it was folded under the influence of a force to re-shape it as a horseshoe, as if its two ends were meeting (b). In this state, when the force was removed after cooling to 25 °C, OHG fixed this temporary shape. OHGs can fix their temporary shape by the hydrophobic interactions of C18A crystals in their

micrometer-sized pores, which were reversibly cracked up when the temperature was increased and were regenerated when the temperature decreased.

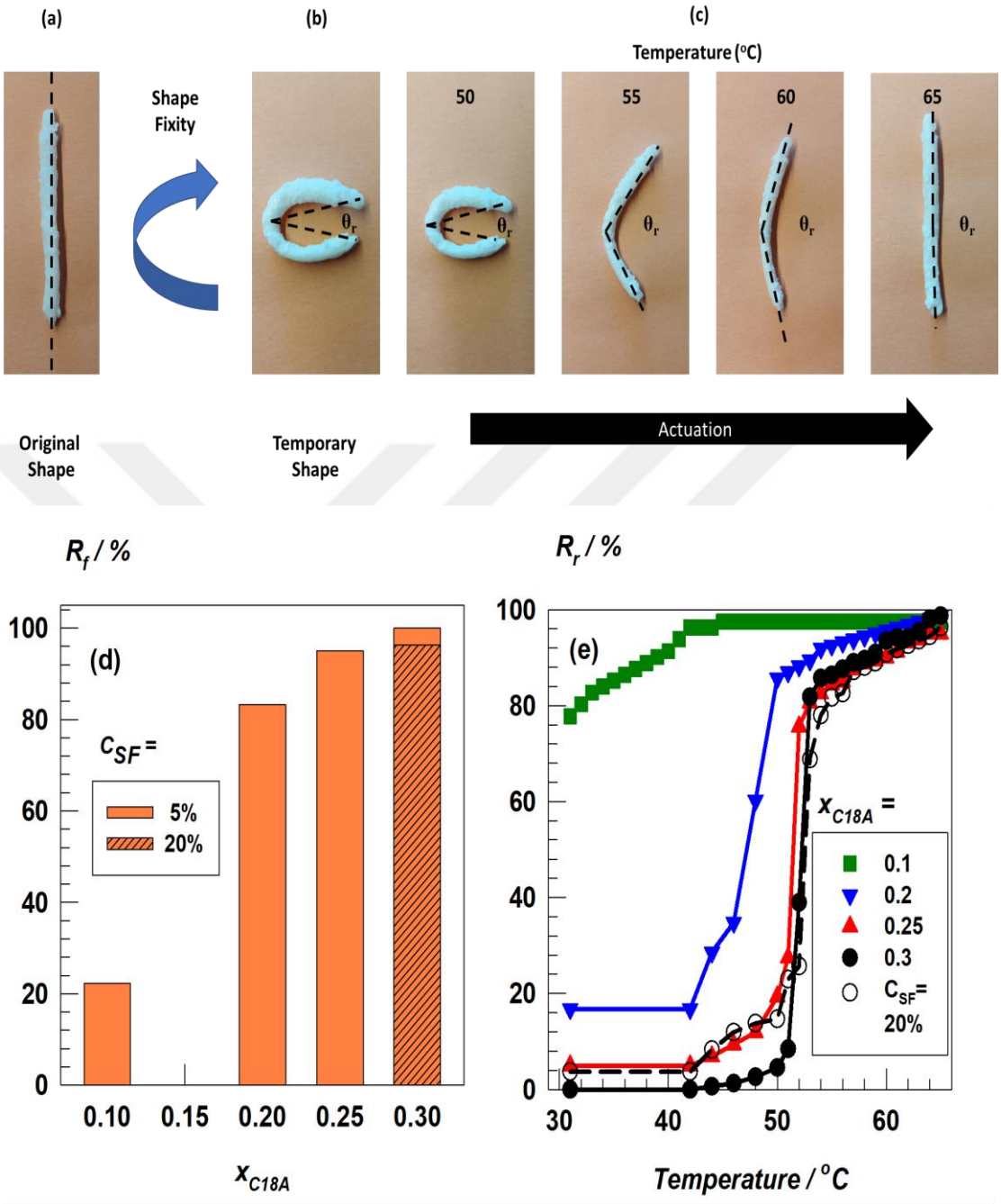

Figure 4.13: (a-c) Shape fixity and recovery behavior of OHG with 5 w/v% C_{SF} and 0.3 x_{C18A} (d-e) Variations of shape fixation R_f and shape recovery R_r rates plotted against x_{C18A} and temperature, respectively. θ_d, θ_f, and θ_r represent the deformation angle under force, the fixed angle after the force is removed, and the recovery angles during heating, respectively. Dashed bar represents the R_r of OHG with 20 w/v% C_{SF} and 0.3 x_{C18A}.

When this temporary shape is heated and no external intervention is made, the cryogel scaffold regains its main shape (straight rod) as a result of returning to their initial configuration as a result of entropic elasticity (Fig. 4.13c).

Figure 4.13d and 4.13e show the shape fixation (R_f) and shape recovery (R_r) values of OHGs as a function of x_{C18A} and temperature, respectively. These values are defined using equation (4.3) and equation (4.4), respectively.

$$R_f = \frac{\theta_f - 180}{\theta_d - 180} \tag{4.3}$$

$$R_r = \frac{\theta_d - \theta_r}{\theta_d - 180} \tag{4.4}$$

Here θ_d, θ_f and θ_r represent the deformation angle of the heated OHG under force, the fixed angle when cooled and the force removed, and the angle recovered after reheating, respectively.

The increase in R_f value with increasing x_{C18A} (Figure 4.13d) revealed that the increased crystallinity of OHG improved its ability to fix the temporary shape. Here all x_{C18A} values are scanned for OHGs with constant 5 w/v% C_{SF} and increasing x_{C18A}. The OHG at the highest x_{C18A} value can completely fix the given temporary shape. Also, for comparison with regard to C_{SF} influence, OHG with 20 w/v% C_{SF} and 0.1 x_{C18A} was also tested, and the R_f value was found to be slightly below that of OHG with 5 w/v% C_{SF} and 0.3 x_{C18A}. For all OHGs, the R_r value is over 95% at 65 °C (Figure 4.14e).

5. CONCLUSIONS

Organohydrogels (OHG), which are nature-inspired amphiphilic functional soft materials, are promising in many applications such as sensors, freeze-resistant materials, drug delivery systems, soft robotics and actuators. In this study, a new and effective approach has been developed for the synthesis of OHGs with programmable mechanical and viscoelastic properties. In this approach, macroporous silk fibroin (SF) cryogel scaffolds of various porosities were used as the hydrophilic continuous phase of the OHGs. The macropores of the cryogels were filled with organogel precursor solution containing C18A, AAc, BAAm, and AIBN. Free-radical polymerization within the pores of the cryogels resulted in the formation of OHGs with tunable mechanical and viscoelastic properties.SF cryogels were produced by cryogelation reactions performed at -18 ^{o}C with the method previously reported in our research group. These cryogel scaffolds were synthesized at 4 different SF concentrations (C_{SF}) of 5, 10, 15 and 20 w/v%, in order to examine the effect of SF concentration on porosity. The organogel structure was synthesized using a gel precursor system containing a covalent crosslinking agent and a thermal radical initiator, using a hydrophilic monomer (AAc) as well as a hydrophobic monomer (C18A) to form crystalline regions. Poly(AAc-co-C18A) organogel was synthesized in the pores of SF cryogels of different concentrations, whose interconnected μm-sized pores were emptied with a freeze dryer, in this ethanolic organogel precursor solution containing AAc, C18A, BAAm and AIBN. The crystalline regions in the OHG structure are formed by C18A comonomer blocks that form hydrophobic interactions with the alkyl side chains of the organogel chains they constituted. In order to show the effect of OHG on the degree of crystallization (f_{cry}) and to examine the effects of this crystallization on thermal, mechanical and viscoelastic properties, and shape memory ability, OHG production was made using organogel precursors of 4 different C18A mole fractions (x_{C18A}) 0.1, 0.2, 0.25 and 0.3 were filled into SF cryogels.

The porosity of the cryogel scaffolds decreased from 92.7 to 74 % with increasing C_{SF}. SEM imaging and swelling tests showed that average pore diameter decreases from 25.71 ± 8.2 to 16.72 ± 4.2 μm, total pore volume (V_p) from 17.4 ± 1.1 to 2. 87 ± 0.7 ml.g^{-1} with increasing C_{SF}. On the other hand, the mechanical properties of cryogels improved gradually, Young's modulus (E) increased from 0.04 to 0.52 MPa and toughness (W) values increased from 0.2 to 0.34 MJ.m^{-3}.As a result of micro-organogel synthesis within the pores, there was a remarkable improvement in mechanical properties compared to the initial cryogel stage. For example, E values of OHGs were measured as approximately 26 times higher than that of cryogels, and W values of approximately 27 times. It was determined that both increasing x_{C18A} and increasing C_{SF} in OHGs increased the E, W and fracture stress values, and the fracture strain remained at around 80% even though it decreased slowly. These superior mechanical characteristics of OHGs compared to the individual properties of their constituents (organogel and cryogel) are due to the efficient energy dissipation mechanism created in their biphasic structure. This energy dissipation mechanism is due to the fact that the cryogel continuous phase helps to maintain mechanical integrity, while the organogel discontinuous phase provides energy damping by micro-fractures. In addition to changing the mechanical properties of OHG at different rates with the changing mole fraction of C18A, the melting point (T_m) and degree of crystallization (f_{cry}) of the semi-crystalline micro-organogel structure are also varied between 41.8 - 53.7 ^{o}C and 2 – 15.7%, respectively. For OHGs with constant 0.3 x_{C18A} and increasing C_{SF}, it was calculated that while the T_m value did not change with the increasing C_{SF} effect, the f_{cry} value decreased in the range of 15.7% - 2.9%. This reduction is due to the difficulty of oriented C18A side chains to form crystalline regions within the cryogel pores getting narrower. These crystalline regions of OHGs give them shape memory capabilities as well as adjustable mechanical and viscoelastic properties that vary under and above T_m temperature. These C18A crystallites were also determined with X-Ray Diffraction (XRD) measurements from the sharp peaks indicated at 2θ = 21.6^{o}. All OHGs have been shown to have a shape recovery of over 95%. In this respect, these OHGs developed within the scope of the study are thought to be suitable for use in tissue engineering, soft robotics, sustained drug release systems and space applications. In addition, this method is a method that can be recommended to be used in the production of OHG, in the heteronetworked approach of OHG production.

REFERENCES

[1] Kim, H., Jeong, H., Han, S., Beack, S., Hwang, B. W., Shin, M., Oh, S. S., & Hahn, S. K. (2017). Hyaluronate and its derivatives for customized biomedical applications. *Biomaterials*, *123*, 155–171. https://doi.org/10.1016/j.biomaterials.2017.01.029

[2] Galler, K. M., Aulisa, L., Regan, K. R., D'Souza, R. N., & Hartgerink, J. D. (2010). Self-Assembling Multidomain Peptide Hydrogels: Designed Susceptibility to Enzymatic Cleavage Allows Enhanced Cell Migration and Spreading. *Journal of the American Chemical Society*, *132*(9), 3217–3223. https://doi.org/10.1021/ja910481t

[3] Levental, I., Georges, P. C., & Janmey, P. A. (2007). Soft biological materials and their impact on cell function. *Soft Matter*, *3*(3), 299–306. https://doi.org/10.1039/B610522J

[4] Peppas, N. A., Hilt, J. Z., Khademhosseini, A., & Langer, R. (2006). Hydrogels in Biology and Medicine: From Molecular Principles to Bionanotechnology. *Advanced Materials*, *18*(11), 1345–1360. https://doi.org/10.1002/adma.200501612

[5] Hoare, T. R., & Kohane, D. S. (2008). Hydrogels in drug delivery: Progress and challenges. *Polymer*, *49*(8), 1993–2007. https://doi.org/10.1016/j.polymer.2008.01.027

[6] Zhao, B., & Moore, J. S. (2001). Fast pH- and Ionic Strength-Responsive Hydrogels in Microchannels. *Langmuir*, *17*(16), 4758–4763. https://doi.org/10.1021/la001709m

[7] Schmaljohann, D., Oswald, J., Jørgensen, B., Nitschke, M., Beyerlein, D., & Werner, C. (2003). Thermo-Responsive PNiPAAm- *g* -PEG Films for Controlled Cell Detachment. *Biomacromolecules*, *4*(6), 1733–1739. https://doi.org/10.1021/bm034160p

[8] Matsumoto, S., Yamaguchi, S., Wada, A., Matsui, T., Ikeda, M., & Hamachi, I. (2008). Photo-responsive gel droplet as a nano- or pico-litre container comprising a supramolecular hydrogel. *Chemical Communications*, *13*, 1545. https://doi.org/10.1039/b719004b

[9] Doi, M., Matsumoto, M., & Hirose, Y. (1992). Deformation of ionic polymer gels by electric fields. *Macromolecules*, *25*(20), 5504–5511. https://doi.org/10.1021/ma00046a058

[10] Zhang, Z., Wang, X., Wang, Y., & Hao, J. (2018). Rapid-Forming and Self-Healing Agarose-Based Hydrogels for Tissue Adhesives and Potential Wound Dressings. *Biomacromolecules*, *19*(3), 980–988. https://doi.org/10.1021/acs.biomac.7b01764

[11] Lu, W., Le, X., Zhang, J., Huang, Y., & Chen, T. (2017). Supramolecular shape memory hydrogels: a new bridge between stimuli-responsive polymers and supramolecular chemistry. *Chemical Society Reviews*, *46*(5), 1284–1294. https://doi.org/10.1039/C6CS00754F

[12] Guo, W., Lu, C.-H., Orbach, R., Wang, F., Qi, X.-J., Cecconello, A., Seliktar, D., & Willner, I. (2015). pH-Stimulated DNA Hydrogels Exhibiting Shape-Memory Properties. *Advanced Materials*, *27*(1), 73–78. https://doi.org/10.1002/adma.201403702

[13] Kato, M., Ito, H., Hasegawa, M., & Ishii, K. (2019). Soft Crystals: Flexible Response Systems with High Structural Order. *Chemistry – A European Journal*, *25*(20), 5105–5112. https://doi.org/10.1002/chem.201805641

[14] Kim, J., Yoon, J., & Hayward, R. C. (2010). Dynamic display of biomolecular patterns through an elastic creasing instability of stimuli-responsive hydrogels. *Nature Materials*, *9*(2), 159–164. https://doi.org/10.1038/nmat2606

[15] HAN L., , WANG S., WANG J., , WANG L., & HE X. (2017). Real-time collection and storage of multi-sensor dynamic parameters. *Chinese Journal of Liquid Crystals and Displays*, *32*(5), 372–379. https://doi.org/10.3788/YJYXS20173205.0372

[16] Pojanavaraphan, T., Liu, L., Ceylan, D., Okay, O., Magaraphan, R., & Schiraldi, D. A. (2011). Solution Cross-Linked Natural Rubber (NR)/Clay Aerogel Composites. *Macromolecules*, *44*(4), 923–931. https://doi.org/10.1021/ma102443k

[17] Abdurrahmanoglu, S., & Okay, O. (2010). Rheological behavior of polymer-clay nanocomposite hydrogels: Effect of nanoscale interactions. *Journal of Applied Polymer Science*, NA-NA. https://doi.org/10.1002/app.31705

[18] Yetiskin, B., Tureyen, O. E., Yilmaz, A., Yakan, S. D., Okay, O. S., & Okay, O. (2019). Single-, Double-, and Triple-Network Macroporous Rubbers as a Passive Sampler. *ACS Applied Materials & Interfaces*, *11*(31), 28317–28326. https://doi.org/10.1021/acsami.9b08788

[19] Yetiskin, B., Akinci, C., & Okay, O. (2017). Cryogelation within cryogels: Silk fibroin scaffolds with single-, double- and triple-network structures. *Polymer*, *128*, 47–56. https://doi.org/10.1016/j.polymer.2017.09.023

[20] Yang, C., & Suo, Z. (2018). Hydrogel ionotronics. *Nature Reviews Materials*, *3*(6), 125–142. https://doi.org/10.1038/s41578-018-0018-7

[21] Gao, S., Sun, J., Liu, P., Zhang, F., Zhang, W., Yuan, S., Li, J., & Jin, J. (2016). A Robust Polyionized Hydrogel with an Unprecedented Underwater Anti-Crude-Oil-Adhesion Property. *Advanced Materials*, *28*(26), 5307–5314. https://doi.org/10.1002/adma.201600417

[22] Liu, M., & Jiang, L. (2016). Dialectics of nature in materials science: binary cooperative complementary materials. *Science China Materials*, *59*(4), 239–246. https://doi.org/10.1007/s40843-016-5051-6

[23] Su, B., Guo, W., & Jiang, L. (2015). Learning from Nature: Binary Cooperative Complementary Nanomaterials. *Small*, *11*(9–10), 1072–1096. https://doi.org/10.1002/smll.201401307

[24] Toxopeus, J., & Sinclair, B. J. (2018). Mechanisms underlying insect freeze tolerance. *Biological Reviews*, *93*(4), 1891–1914. https://doi.org/10.1111/brv.12425

[25] Thomashow, M. F. (1999). PLANT COLD ACCLIMATION: Freezing Tolerance Genes and Regulatory Mechanisms. *Annual Review of Plant Physiology and Plant Molecular Biology*, *50*(1), 571–599. https://doi.org/10.1146/annurev.arplant.50.1.571

[26] Capadona, J. R., Shanmuganathan, K., Tyler, D. J., Rowan, S. J., & Weder, C. (2008). Stimuli-Responsive Polymer Nanocomposites Inspired by the Sea Cucumber Dermis. *Science*, *319*(5868), 1370–1374. https://doi.org/10.1126/science.1153307

[27] Thurmond, F., & Trotter, J. (1996). Morphology and biomechanics of the microfibrillar network of sea cucumber dermis. *Journal of Experimental Biology*, *199*(8), 1817–1828. https://doi.org/10.1242/jeb.199.8.1817

[28] Tepic, S., Macirowski, T., & Mann, R. W. (1983). Mechanical properties of articular cartilage elucidated by osmotic loading and ultrasound. *Proceedings of the National Academy of Sciences*, *80*(11), 3331–3333. https://doi.org/10.1073/pnas.80.11.3331

[29] Jana, S., Levengood, S. K. L., & Zhang, M. (2016). Anisotropic Materials for Skeletal-Muscle-Tissue Engineering. *Advanced Materials*, *28*(48), 10588–10612. https://doi.org/10.1002/adma.201600240

[30] Gao, W., Lei, Z., Zhang, C., Liu, X., & Chen, Y. (2021). Stretchable and Freeze-Tolerant Organohydrogel Thermocells with Enhanced Thermoelectric Performance Continually Working at Subzero Temperatures. *Advanced Functional Materials*, *31*(43), 2104071. https://doi.org/10.1002/adfm.202104071

[31] Zhao, Z., Zhang, K., Liu, Y., Zhou, J., & Liu, M. (2017). Highly Stretchable, Shape Memory Organohydrogels Using Phase-Transition Microinclusions. *Advanced Materials*, *29*(33), 1701695. https://doi.org/10.1002/adma.201701695

[32] Jian, Y., Wu, B., Le, X., Liang, Y., Zhang, Y., Zhang, D., Zhang, L., Lu, W., Zhang, J., & Chen, T. (2019). Antifreezing and Stretchable Organohydrogels as Soft Actuators. *Research*, *2019*, 1–11. https://doi.org/10.34133/2019/2384347

[33] Zhao, Z., Li, C., Dong, Z., Yang, Y., Zhang, L., Zhuo, S., Zhou, X., Xu, Y., Jiang, L., & Liu, M. (2019). Adaptive Superamphiphilic Organohydrogels with Reconfigurable Surface Topography for Programming Unidirectional Liquid Transport. *Advanced Functional Materials*, *29*(16), 1807858. https://doi.org/10.1002/adfm.201807858

[34] Hanay, S. B., O'Dwyer, J., Kimmins, S. D., de Oliveira, F. C. S., Haugh, M. G., O'Brien, F. J., Cryan, S.-A., & Heise, A. (2018). Facile Approach

to Covalent Copolypeptide Hydrogels and Hybrid Organohydrogels. *ACS Macro Letters*, *7*(8), 944–949. https://doi.org/10.1021/acsmacrolett.8b00431

[35] Pan, X., Wang, Q., Ning, D., Dai, L., Liu, K., Ni, Y., Chen, L., & Huang, L. (2018). Ultraflexible Self-Healing Guar Gum-Glycerol Hydrogel with Injectable, Antifreeze, and Strain-Sensitive Properties. *ACS Biomaterials Science and Engineering*, *4*(9), 3397–3404. https://doi.org/10.1021/ACSBIOMATERIALS.8B00657/ASSET/IMAGES/MEDIUM/AB-2018-00657J_0011.GIF

[36] Chen, F., Zhou, D., Wang, J., Li, T., Zhou, X., Gan, T., Handschuh-Wang, S., & Zhou, X. (2018). Rational Fabrication of Anti-Freezing, Non-Drying Tough Organohydrogels by One-Pot Solvent Displacement. *Angewandte Chemie*, *130*(22), 6678–6681. https://doi.org/10.1002/ange.201803366

[37] He, Z., & Yuan, W. (2021). Adhesive, Stretchable, and Transparent Organohydrogels for Antifreezing, Antidrying, and Sensitive Ionic Skins. *ACS Applied Materials & Interfaces*, *13*(1), 1474–1485. https://doi.org/10.1021/acsami.0c18405

[38] Chen, X., Liu, L., Liu, K., Miao, Q., Lü, Y., & Fang, Y. (2015). Compressible porous hybrid monoliths: preparation via a low molecular mass gelators-based gel-emulsion approach and exceptional performances. *Journal of Materials Chemistry A*, *3*(48), 24322–24332. https://doi.org/10.1039/C5TA08342G

[39] Okay, O. (Ed.). (2014). *Polymeric Cryogels* (Vol. 263). Springer International Publishing. https://doi.org/10.1007/978-3-319-05846-7

[40] Lozinsky, V. I., & Okay, O. (2014). *Basic Principles of Cryotropic Gelation* (pp. 49–101). https://doi.org/10.1007/978-3-319-05846-7_2

[41] Ak, F., Oztoprak, Z., Karakutuk, I., & Okay, O. (2013). Macroporous Silk Fibroin Cryogels. *Biomacromolecules*, *14*(3), 719–727. https://doi.org/10.1021/bm3018033

[42] Babu, K. M. (2020). Silk fibres – structure, properties and applications. In *Handbook of Natural Fibres* (pp. 385–416). Elsevier. https://doi.org/10.1016/B978-0-12-818398-4.00013-X

[43] Dinjaski, N., & Kaplan, D. L. (2016). Recombinant protein blends: silk beyond natural design. *Current Opinion in Biotechnology*, *39*, 1–7. https://doi.org/10.1016/j.copbio.2015.11.002

[44] Scheibel, T. (2004). Spider silks: recombinant synthesis, assembly, spinning, and engineering of synthetic proteins. *Microbial Cell Factories*, *3*(1), 14. https://doi.org/10.1186/1475-2859-3-14

[45] Holland, C., Numata, K., Rnjak-Kovacina, J., & Seib, F. P. (2019). The Biomedical Use of Silk: Past, Present, Future. *Advanced Healthcare Materials*, *8*(1), 1800465. https://doi.org/10.1002/adhm.201800465

[46] Mondal, M., Trivedy, K., & Nirmal Kumar, S. (2007). The silk proteins, sericin and fibroin in silkworm, Bombyx mori Linn.,-a review. In *Caspian*

Journal of Environmental Sciences Caspian J. Env. Sci (Vol. 5, Issue 2). http://research.guilan.ac.ir/cjesorwww.cjes.net

[47] Vepari, C., & Kaplan, D. L. (2007). Silk as a biomaterial. *Progress in Polymer Science*, *32*(8–9), 991–1007. https://doi.org/10.1016/j.progpolymsci.2007.05.013

[48 Zhou, C.-Z., Confalonieri, F., Jacquet, M., Perasso, R., Li, Z.-G., & Janin, J. (2001). Silk fibroin: Structural implications of a remarkable amino acid sequence. *Proteins: Structure, Function, and Genetics*, *44*(2), 119–122. https://doi.org/10.1002/prot.1078

[49] Galler, K. M., Aulisa, L., Regan, K. R., D'Souza, R. N., & Hartgerink, J. D. (2010). Self-Assembling Multidomain Peptide Hydrogels: Designed Susceptibility to Enzymatic Cleavage Allows Enhanced Cell Migration and Spreading. *Journal of the American Chemical Society*, *132*(9), 3217–3223. https://doi.org/10.1021/ja910481t

[50] Sarkar, A., Connor, A. J., Koffas, M., & Zha, R. H. (2019). Chemical Synthesis of Silk-Mimetic Polymers. *Materials*, *12*(24), 4086. https://doi.org/10.3390/ma12244086

[51] Motta, A., Migliaresi, C., Faccioni, F., Torricelli, P., Fini, M., & Giardino, R. (2012). Fibroin hydrogels for biomedical applications: preparation, characterization and in vitro cell culture studies. *Https://Doi.Org/10.1163/1568562041271075*, *15*(7), 851–864. https://doi.org/10.1163/1568562041271075

[52] Matsumoto, A., Chen, J., Collette, A. L., Kim, U.-J., Altman, G. H., Cebe, P., & Kaplan, D. L. (2006). Mechanisms of Silk Fibroin Sol−Gel Transitions. *The Journal of Physical Chemistry B*, *110*(43), 21630–21638. https://doi.org/10.1021/jp056350v

[53] Um, I. C., Kweon, H. Y., Lee, K. G., & Park, Y. H. (2003). The role of formic acid in solution stability and crystallization of silk protein polymer. *International Journal of Biological Macromolecules*, *33*(4–5), 203–213. https://doi.org/10.1016/j.ijbiomac.2003.08.004

[54] Ayub, Z. H., Arai, M., & Hirabayashi, K. (1993). Mechanism of the Gelation of Fibroin Solution. *Bioscience, Biotechnology, and Biochemistry*, *57*(11), 1910–1912. https://doi.org/10.1271/bbb.57.1910

[55] Lu, X., Xu, Y., Zheng, C., Zhang, G., & Su, Z. (2006). Ethylene glycol diglycidyl ether as a protein cross-linker: a case study for cross-linking of hemoglobin. *Journal of Chemical Technology & Biotechnology*, *81*(5), 767–775. https://doi.org/10.1002/jctb.1441

[56] Tanaka, T. (1981). Gels. *Scientific American*, *244*(1), 124–138. https://doi.org/10.1038/scientificamerican0181-124

[57] Ganguly, S., Das, P., & Das, N. Ch. (2020). Characterization tools and techniques of hydrogels. In *Hydrogels Based on Natural Polymers* (pp. 481–517). Elsevier. https://doi.org/10.1016/B978-0-12-816421-1.00016-1

[58] Okay, O. (2009). *General Properties of Hydrogels* (pp. 1–14). https://doi.org/10.1007/978-3-540-75645-3_1

[59] Li, Z., Zhou, Y., Li, T., Zhang, J., & Tian, H. (2022). Stimuli-responsive hydrogels: Fabrication and biomedical applications. *VIEW*, *3*(2), 20200112. https://doi.org/10.1002/VIW.20200112

[60] Shibayama, M., & Tanaka, T. (1993). *Volume phase transition and related phenomena of polymer gels* (pp. 1–62). https://doi.org/10.1007/3-540-56791-7_1

[61] Oh, K. k. (1998). Effect of Crosslinking Density on Swelling Behavior of NIPA Gel Particles. *Macromolecules.*, *31*(21), 7328–7335.

[62] Yoshida, R., Uchida, K., Kaneko, Y., Sakai, K., Kikuchi, A., Sakurai, Y., & Okano, T. (1995). Comb-type grafted hydrogels with rapid deswelling response to temperature changes. *Nature*, *374*(6519), 240–242. https://doi.org/10.1038/374240a0

[63] Guo, Y., Vasconcelos, L. S., Manohar, N., Geng, J., Johnston, K. P., & Yu, G. (2022). Highly Elastic Interconnected Porous Hydrogels through Self-Assembled Templating for Solar Water Purification. *Angewandte Chemie International Edition*, *61*(3). https://doi.org/10.1002/anie.202114074

[64] Lozinsky, V. I. (2002). Cryogels on the basis of natural and synthetic polymers: preparation, properties and application. *Russian Chemical Reviews*, *71*(6), 489–511. https://doi.org/10.1070/RC2002v071n06ABEH000720

[65] Eggermont, L. J., Rogers, Z. J., Colombani, T., Memic, A., & Bencherif, S. A. (2020). Injectable Cryogels for Biomedical Applications. *Trends in Biotechnology*, *38*(4), 418–431. https://doi.org/10.1016/j.tibtech.2019.09.008

[66] Yetiskin, B., & Okay, O. (2019). High-strength and self-recoverable silk fibroin cryogels with anisotropic swelling and mechanical properties. *International Journal of Biological Macromolecules*, *122*, 1279–1289. https://doi.org/10.1016/j.ijbiomac.2018.09.087

[67] Dragan, E. S., Humelnicu, D., & Dinu, M. V. (2019). Development of chitosan-poly(ethyleneimine) based double network cryogels and their application as superadsorbents for phosphate. *Carbohydrate Polymers*, *210*, 17–25. https://doi.org/10.1016/j.carbpol.2019.01.054

[68] Loo, S.-L., Fane, A. G., Lim, T.-T., Krantz, W. B., Liang, Y.-N., Liu, X., & Hu, X. (2013). Superabsorbent Cryogels Decorated with Silver Nanoparticles as a Novel Water Technology for Point-of-Use Disinfection. *Environmental Science & Technology*, *47*(16), 9363–9371. https://doi.org/10.1021/es401219s

[69] Zainol, M. M., Amin, N. A. S., & Asmadi, M. (2019). Kinetics and thermodynamic analysis of levulinic acid esterification using lignin-furfural carbon cryogel catalyst. *Renewable Energy*, *130*, 547–557. https://doi.org/10.1016/j.renene.2018.06.085

[70] Sahiner, N., Seven, F., & Al-Lohedan, H. (2015). Super-fast hydrogen generation via super porous Q-P(VI)-M cryogel catalyst systems from

hydrolysis of NaBH4. *International Journal of Hydrogen Energy*, *40*(13), 4605–4616. https://doi.org/10.1016/j.ijhydene.2015.02.049

[71] Demir, D., Vaseashta, A., & Bölgen, N. (2021). *Macroporous Cryogels for Water Purification* (pp. 275–290). https://doi.org/10.1007/978-3-030-76008-3_12

[72] Saylan, & Denizli. (2019). Supermacroporous Composite Cryogels in Biomedical Applications. *Gels*, *5*(2), 20. https://doi.org/10.3390/gels5020020

[73] Kempaiah, R., & Nie, Z. (2014). From nature to synthetic systems: shape transformation in soft materials. *J. Mater. Chem. B*, *2*(17), 2357–2368. https://doi.org/10.1039/C3TB21462A

[74] Bellamkonda, R. v. (2008). Marine inspiration. *Nature Materials*, *7*(5), 347–348. https://doi.org/10.1038/nmat2176

[75] Wang, Y., Cui, H., Zhao, Q., & Du, X. (2019). Chameleon-Inspired Structural-Color Actuators. *Matter*, *1*(3), 626–638. https://doi.org/10.1016/j.matt.2019.05.012

[76] Liu, C., Qin, H., & Mather, P. T. (2007). Review of progress in shape-memory polymers. *Journal of Materials Chemistry*, *17*(16), 1543. https://doi.org/10.1039/b615954k

[77] Yang, X. (2001). Conformational elasticity theory of chain molecules. *Science in China Series B: Chemistry*, *44*(2), 154–168. https://doi.org/10.1007/BF02879533

[78] Liu, F., & Urban, M. W. (2010). Recent advances and challenges in designing stimuli-responsive polymers. *Progress in Polymer Science*, *35*(1–2), 3–23. https://doi.org/10.1016/j.progpolymsci.2009.10.002

[79] Liu, C., Chun, S. B., Mather, P. T., Zheng, L., Haley, E. H., & Coughlin, E. B. (2002). Chemically Cross-Linked Polycyclooctene: Synthesis, Characterization, and Shape Memory Behavior. *Macromolecules*, *35*(27), 9868–9874. https://doi.org/10.1021/ma021141j

[80] Balk, M., Behl, M., & Lendlein, A. (2019). Quadruple-shape hydrogels. *Smart Materials and Structures*, *28*(5), 055026. https://doi.org/10.1088/1361-665X/ab0e91

[81] Behl, M., & Lendlein, A. (2010). Triple-shape polymers. *Journal of Materials Chemistry*, *20*(17), 3335. https://doi.org/10.1039/b922992b

[82] Zhang, Z., & Hao, J. (2021). Bioinspired organohydrogels with heterostructures: Fabrications, performances, and applications. *Advances in Colloid and Interface Science*, *292*, 102408. https://doi.org/10.1016/j.cis.2021.102408

[83] Zhao, T., Wang, G., Hao, D., Chen, L., Liu, K., & Liu, M. (2018). Macroscopic Layered Organogel-Hydrogel Hybrids with Controllable Wetting and Swelling Performance. *Advanced Functional Materials*, *28*(49), 1800793. https://doi.org/10.1002/adfm.201800793

[84] Li, C., Feng, S., Li, C., Sui, Y., Shen, J., Huang, C., Wu, Y., & Huang, W. (2020). Synthesizing Organo/Hydrogel Hybrids with Diverse

Programmable Patterns and Ultrafast Self-Actuating Ability via a Site-Specific “In Situ” Transformation Strategy. *Advanced Functional Materials*, *30*(32), 2002163. https://doi.org/10.1002/adfm.202002163

[85] Han, L., Liu, K., Wang, M., Wang, K., Fang, L., Chen, H., Zhou, J., & Lu, X. (2018). Mussel-Inspired Adhesive and Conductive Hydrogel with Long-Lasting Moisture and Extreme Temperature Tolerance. *Advanced Functional Materials*, *28*(3), 1704195. https://doi.org/10.1002/adfm.201704195

[86] Liu, J., Li, M., Wang, P., Liu, K., & Fang, Y. (2018). Gel-emulsion templated polymeric monoliths for efficient removal of particulate matters. *Chemical Engineering Journal*, *339*, 14–21. https://doi.org/10.1016/J.CEJ.2018.01.110

[87] Miao, Q., Chen, X., Liu, L., Peng, J., & Fang, Y. (2014). Synergetic Effect Based Gel-Emulsions and Their Utilization for the Template Preparation of Porous Polymeric Monoliths. *Langmuir*, *30*(45), 13680–13688. https://doi.org/10.1021/la502988x

[88] Chen, X., Liu, K., He, P., Zhang, H., & Fang, Y. (2012). Preparation of Novel W/O Gel-Emulsions and Their Application in the Preparation of Low-Density Materials. *Langmuir*, *28*(25), 9275–9281. https://doi.org/10.1021/la300856h

[89] Peng, J., Xia, H., Liu, K., Gao, D., Yang, M., Yan, N., & Fang, Y. (2009). Water-in-oil gel emulsions from a cholesterol derivative: Structure and unusual properties. *Journal of Colloid and Interface Science*, *336*(2), 780–785. https://doi.org/10.1016/J.JCIS.2009.04.055

[90] Zhuo, S., Zhao, Z., Xie, Z., Hao, Y., Xu, Y., Zhao, T., Li, H., Knubben, E. M., Wen, L., Jiang, L., & Liu, M. (2020). Complex multiphase organohydrogels with programmable mechanics toward adaptive soft-matter machines. *Science Advances*, *6*(5). https://doi.org/10.1126/sciadv.aax1464

[91] Panteli, P. A., Patrickios, C. S., Constantinou, M., & Constantinides, G. (2019). Multiple Network Hydrogels: A Study of Their Nanoindentation Hardness. *Macromolecular Symposia*, *385*(1), 1800201. https://doi.org/10.1002/masy.201800201

[92] Gong, J. P., Katsuyama, Y., Kurokawa, T., & Osada, Y. (2003). Double-Network Hydrogels with Extremely High Mechanical Strength. *Advanced Materials*, *15*(14), 1155–1158. https://doi.org/10.1002/adma.200304907

[93] Na, Y. H. (2013). Double network hydrogels with extremely high toughness and their applications. *Korea-Australia Rheology Journal*, *25*(4), 185–196. https://doi.org/10.1007/s13367-013-0020-y

[94] Argun, A., Can, V., Altun, U., & Okay, O. (2014). Nonionic Double and Triple Network Hydrogels of High Mechanical Strength. *Macromolecules*, *47*(18), 6430–6440. https://doi.org/10.1021/ma5014176

[95] Gao, H., Cai, Y., Li, S., Zhang, X., Zhao, T., Liu, M., & Jiang, L. (2020). Heteronetwork organohydrogels with exceptional swelling-resistance and adaptive antifouling performance. *Polymer Chemistry*, *11*(1), 68–74. https://doi.org/10.1039/C9PY01429B

[96] Gao, H., Zhao, Z., Cai, Y., Zhou, J., Hua, W., Chen, L., Wang, L., Zhang, J., Han, D., Liu, M., & Jiang, L. (2017). Adaptive and freeze-tolerant heteronetwork organohydrogels with enhanced mechanical stability over a wide temperature range. *Nature Communications*, *8*(1), 15911. https://doi.org/10.1038/ncomms15911

[97] Yang, Y., Guan, L., Li, X., Gao, Z., Ren, X., & Gao, G. (2019). Conductive Organohydrogels with Ultrastretchability, Antifreezing, Self-Healing, and Adhesive Properties for Motion Detection and Signal Transmission. *ACS Applied Materials & Interfaces*, *11*(3), 3428–3437. https://doi.org/10.1021/acsami.8b17440

[98] Yetiskin, B., & Okay, O. (2022). Silk Fibroin Cryogel Building Adaptive Organohydrogels with Switching Mechanics and Viscoelasticity. *ACS Applied Polymer Materials*, *4*(7), 5234–5245. https://doi.org/10.1021/acsapm.2c00741

[99] Oral, C. B., Yetiskin, B., & Okay, O. (2020). Stretchable silk fibroin hydrogels. *International Journal of Biological Macromolecules*, *161*, 1371–1380. https://doi.org/10.1016/j.ijbiomac.2020.08.040

[100] Okay, O. (2000). Macroporous copolymer networks. *Progress in Polymer Science*, *25*(6), 711–779. https://doi.org/10.1016/S0079-6700(00)00015-0

[101] Su, E., Bilici, C., Bayazit, G., Ide, S., & Okay, O. (2021). Solvent-Free UV Polymerization of *n* -Octadecyl Acrylate in Butyl Rubber: A Simple Way to Produce Tough and Smart Polymeric Materials at Ambient Temperature. *ACS Applied Materials & Interfaces*, *13*(18), 21786–21799. https://doi.org/10.1021/acsami.1c03814

[102] Okay, O., & Lozinsky, V. I. (2014). *Synthesis and Structure–Property Relationships of Cryogels* (pp. 103–157). https://doi.org/10.1007/978-3-319-05846-7_3

[103] Okay, O. (2019). Semicrystalline physical hydrogels with shape-memory and self-healing properties. *Journal of Materials Chemistry B*, *7*(10), 1581–1596. https://doi.org/10.1039/C8TB02767F

[104] Kurt, B., Gulyuz, U., Demir, D. D., & Okay, O. (2016). High-strength semi-crystalline hydrogels with self-healing and shape memory functions. *European Polymer Journal*, *81*, 12–23. https://doi.org/10.1016/j.eurpolymj.2016.05.019

[105] Bilici, C., Can, V., Nöchel, U., Behl, M., Lendlein, A., & Okay, O. (2016). Melt-Processable Shape-Memory Hydrogels with Self-Healing Ability of High Mechanical Strength. *Macromolecules*, *49*(19), 7442–7449. https://doi.org/10.1021/acs.macromol.6b01539

[106] Gulyuz, U., & Okay, O. (2015). Self-Healing Poly(acrylic acid) Hydrogels: Effect of Surfactant. *Macromolecular Symposia*, *358*(1), 232–238. https://doi.org/10.1002/masy.201500063

[107] Valluzzi, R., He, S. J., Gido, S. P., & Kaplan, D. (1999). Bombyx mori silk fibroin liquid crystallinity and crystallization at aqueous fibroin–organic solvent interfaces. *International Journal of Biological Macromolecules*, *24*(2–3), 227–236. https://doi.org/10.1016/S0141-8130(99)00005-7

[108] Noishiki, Y., Nishiyama, Y., Wada, M., Kuga, S., & Magoshi, J. (2002). Mechanical properties of silk fibroin-microcrystalline cellulose composite films. *Journal of Applied Polymer Science*, *86*(13), 3425–3429. https://doi.org/10.1002/app.11370

[109] Li, M., Ogiso, M., & Minoura, N. (2003). Enzymatic degradation behavior of porous silk fibroin sheets. *Biomaterials*, *24*(2), 357–365. https://doi.org/10.1016/S0142-9612(02)00326-5

[110] Zhu, Y., Liu, H., Qin, S., Yang, C., Lv, Q., Wang, Z., & Wang, L. (2022). Antibacterial Sericin Cryogels Promote Hemostasis by Facilitating the Activation of Coagulation Pathway and Platelets (Adv. Healthcare Mater. 11/2022). *Advanced Healthcare Materials*, *11*(11), 2270059. https://doi.org/10.1002/adhm.202270059

[111] Dai, R., Meng, L., Fu, Q., Hao, S., & Yang, J. (2021). Fabrication of Anisotropic Silk Fibroin-Cellulose Nanocrystals Cryogels with Tunable Mechanical Properties, Rapid Swelling, and Structural Recoverability via a Directional-Freezing Strategy. *ACS Sustainable Chemistry & Engineering*, *9*(36), 12274–12285. https://doi.org/10.1021/acssuschemeng.1c03852

[112] Shirbin, S. J., Lam, S. J., Chan, N. J.-A., Ozmen, M. M., Fu, Q., O'Brien-Simpson, N., Reynolds, E. C., & Qiao, G. G. (2016). Polypeptide-Based Macroporous Cryogels with Inherent Antimicrobial Properties: The Importance of a Macroporous Structure. *ACS Macro Letters*, *5*(5), 552–557. https://doi.org/10.1021/acsmacrolett.6b00174

[113] Zhou, H., Lai, J., Zheng, B., Jin, X., Zhao, G., Liu, H., Chen, W., Ma, A., Li, X., & Wu, Y. (2022). From Glutinous-Rice-Inspired Adhesive Organohydrogels to Flexible Electronic Devices Toward Wearable Sensing, Power Supply, and Energy Storage. *Advanced Functional Materials*, *32*(1), 2108423. https://doi.org/10.1002/adfm.202108423

[114] Jiang, L., Liu, J., He, S., Liu, A., Zhang, J., Xu, H., & Shao, W. (2022). Flexible wearable sensors based on lignin doped organohydrogels with multi-functionalities. *Chemical Engineering Journal*, *430*, 132653. https://doi.org/10.1016/j.cej.2021.132653

[115] Yu, Q., Qin, Z., Ji, F., Chen, S., Luo, S., Yao, M., Wu, X., Liu, W., Sun, X., Zhang, H., Zhao, Y., Yao, F., & Li, J. (2021). Low-temperature tolerant strain sensors based on triple crosslinked organohydrogels with ultrastretchability. *Chemical Engineering Journal*, *404*, 126559. https://doi.org/10.1016/j.cej.2020.126559

[116] Zhang, Z., Guo, L., Zhang, X., & Hao, J. (2020). Environmentally stable, photochromic and thermotropic organohydrogels for low cost on-demand optical devices. *Journal of Colloid and Interface Science*, *578*, 315–325. https://doi.org/10.1016/j.jcis.2020.05.110

[117] Wu, J., Wu, Z., Xu, H., Wu, Q., Liu, C., Yang, B.-R., Gui, X., Xie, X., Tao, K., Shen, Y., Miao, J., & Norford, L. K. (2019). An intrinsically stretchable humidity sensor based on anti-drying, self-healing and transparent organohydrogels. *Materials Horizons*, *6*(3), 595–603. https://doi.org/10.1039/C8MH01160E

CURRICULUM VITAE

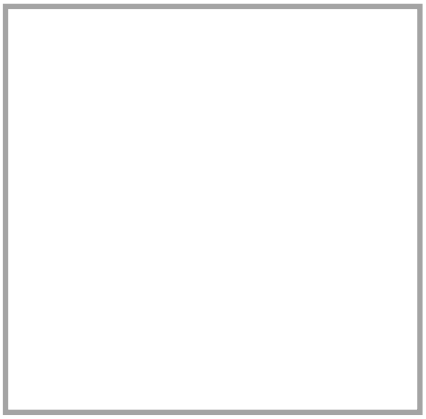

Name-Surname **:** Yahya BAŞ

EDUCATION:

- **B. Sc.** **:** 2019, Istanbul University, F. of Eng., Chemical Engineering
- **M. Sc.** **:** 2022, Istanbul Technical University, Graduate School, Polymer Science and Technologly

PUBLICATIONS, PRESENTATIONS AND PATENTS DERIVED FROM THESIS:

- Baş Y.., 2021. Gözenekleri Mikro-Organojel Yüklü Ve Mekanik Özellikleri Sıcaklık İle Değişebilen Akıllı Fibroin Kriyojelleri. *33rd National Chemistry Symposium*, October 7-9, 2021 Tekirdağ, Turkey.